ChemPubSoc Europe
DOI: 10.1002/chem.201605957
CHEMISTRY A European Journal Review

Nanoparticles

Mechanistic Aspects in the Formation, Growth and Surface Functionalization of Metal Oxide Nanoparticles in Organic Solvents

Rupali Deshmukh and Markus Niederberger*[a]

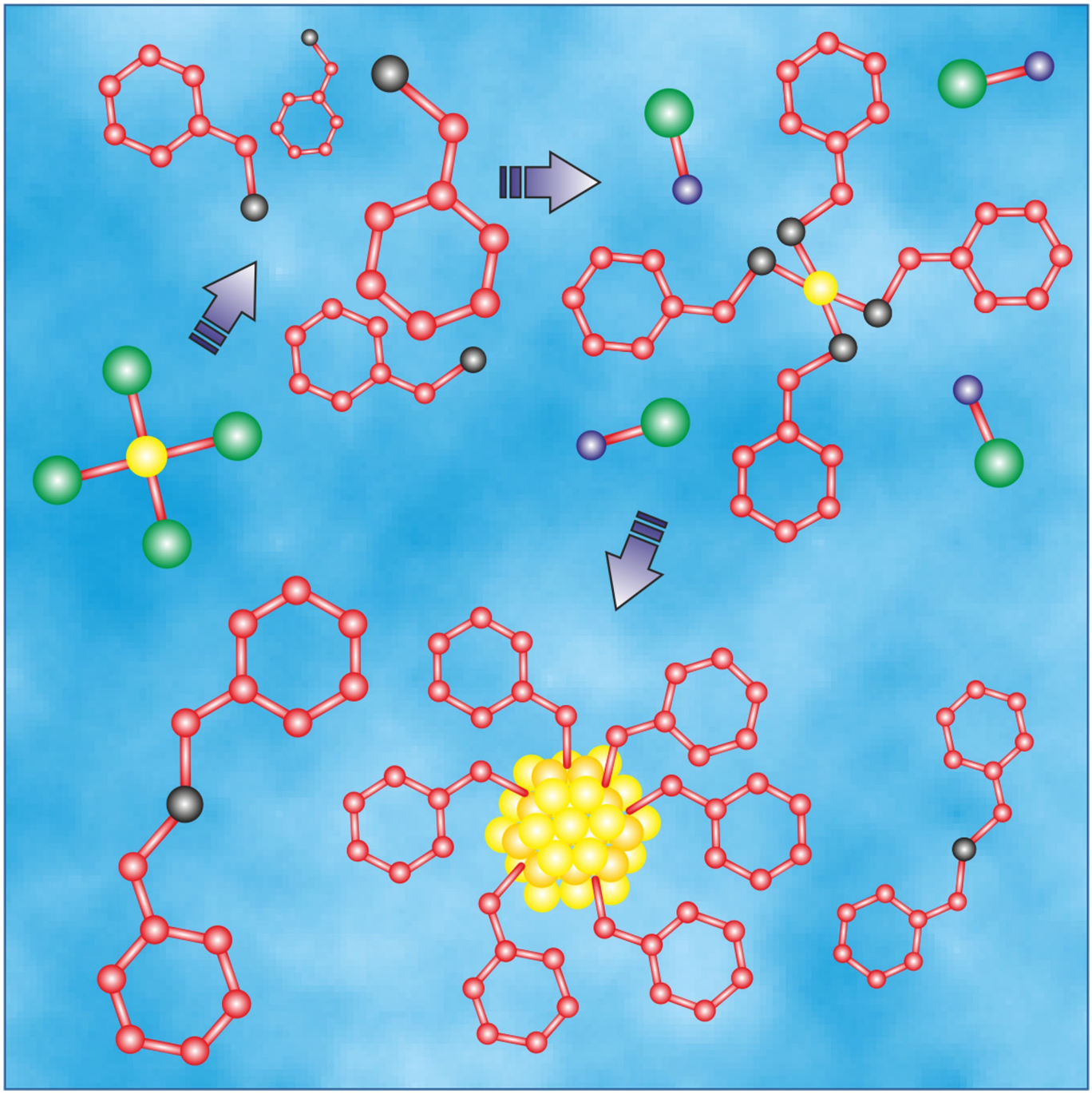

Abstract: The synthesis of metal oxide nanoparticles in organic solvents, so-called nonaqueous (or nonhydrolytic) processes represent powerful alternatives to aqueous approaches and have become an independent research field. 10 Years ago, when we published our first review on organic reaction pathways in nonaqueous sol–gel approaches,[1] the number of examples was relatively limited. Nowadays, it is almost impossible to provide an exhaustive overview. Here we review the development of the last few years, without neglecting pioneering examples, which help to follow the historical development. The importance of a profound understanding of mechanistic aspects of nanoparticle crystallization and formation mechanisms can't be overestimated, when it comes to the design of rational synthesis concepts under minimization of trial-and-error experiments. The main reason for the progress in mechanistic understanding lies in the availability of characterization tools that make it possible to monitor chemical reactions from the dissolution of the precursor to the nucleation and growth of the nanoparticles, by ex situ methods involving sampling after different reaction times, but more and more also by in situ studies. After a short introduction to experimental aspects of nonaqueous sol–gel routes to metal oxide nanoparticles, we provide an overview of the main and basic organic reaction pathways in these approaches. Afterwards, we summarize the main characterization methods to study formation mechanisms, and then we discuss in great depth the chemical formation mechanisms of many different types of metal oxide nanoparticles. The review concludes with a paragraph on selected crystallization mechanisms reported for nonaqueous systems and a few illustrative examples of nonaqueous sol–gel concepts applied to surface chemistry.

1. Introduction

Tailor-made and highly specialized nanomaterials hold the key for fundamental advances in diverse areas such as energy conversion,[2–4] energy storage,[3,5] heterogeneous catalysis,[6–8] data storage,[9] medicine,[10–12] and other industrial applications.[13] Solvent-based synthesis approaches are particularly suitable for nanoparticles, because during the chemical transformation of the homogeneously dissolved molecular precursors into the final products many ways exist to control the particle morphology, the crystallinity and the surface properties, and thus the agglomeration behavior. Such a subtle control is absolutely essential considering that on the nanoscale, size and shape are nearly as important as the composition in determining the chemical and physical properties of materials.[14]

Nowadays many different synthesis approaches (liquid-[15–19] as well as gas-phase routes[20,21]) to a large variety of nanoparticles and nanostructures are available, covering nearly all classes of materials. But in spite of the great progress in nanoparticle synthesis, several major challenges remain. It is impossible to predict the particle morphology from a specific reaction mixture. Surface-functionalization to prevent agglomeration and to enable dispersion for further processing of nanoparticles remains difficult. Reliable and reproducible scale-up from laboratory to industrial quantities is, especially for solution routes, still a problem. Clearly, these issues are connected to a lack of in-depth knowledge about nanoparticle formation and crystallization mechanisms and about their surface chemistry.

The reasons, why mechanistic aspects of nanoparticle formation are not well understood, are not at all due to missing efforts within the scientific community. The high complexity of the reaction pathways and their pronounced chemical sensitivity on slight variations of the synthesis protocols makes it nearly impossible to elaborate generally valid rules and concepts. Moreover, reaction mixtures containing several compounds severely complicate mechanistic studies. Systematic variation of the chemical compounds in the initial reaction mixture and observation of the resulting changes of the product is currently the standard way to elaborate the role of the different chemicals in a synthesis system, and in an increasing number of cases, the studies are supported by modeling.

There are absolutely no doubts that any mechanistic insights are immensely helpful to explain the outcome of a synthesis and to improve the synthesis protocols. Unfortunately, in most of the studies the explanations follow the experimental observations, and the predictive character is strongly limited. Starting from a specific reaction mixture it is still impossible to foresee the composition, the crystal structure and the morphology of the forming nanoparticles considering the influence of all chemical species (initially added, but also formed in situ) as well as of the physical reaction conditions.

Mechanistic studies are tedious, time consuming and labor intensive, because they have to include all aspects of nanoparticle formation, including pre-nucleation processes, nucleation and growth, assembly and agglomeration, chemical reaction pathways and the solid–liquid interface at all stages of the synthesis. In addition, the results have to be put in the context of current theories, and basic concepts have to be widened and adapted to the experimental results. As a matter of fact, experimentally observed "anomalies" have been at the origin of a lively discussion on the mechanism of crystallization for decades.[22,23] Concepts such as pre-nucleation clusters,[24] oriented attachment,[25,26] particle-based crystallization mechanisms[23,27] and mesocrystals[28] helped to explain the experimental observations apparently contradicting the classical view of crystallization. With increasing complexity of the crystallization mechanisms not only the capabilities of dedicated

[a] *Dr. R. Deshmukh, Prof. Dr. M. Niederberger*
Laboratory for Multifunctional Materials, Department of Materials
ETH Zürich, Vladimir-Prelog-Weg 5, 8093 Zürich (Switzerland)
E-mail: markus.niederberger@mat.ethz.ch

The ORCID identification number(s) for the author(s) of this article can be found under https://doi.org/10.1002/chem.201605957.

characterization methods have to be extended,[29] but tools from other research areas have to be adapted to the in situ monitoring of nanoparticle growth.[30] A complete reaction monitoring from the dissolution of the precursor to the formation of the final nanocrystalline product makes greatest demands to the applied probes. Inorganic and organic reactions and compounds as well as solid and liquid interfaces have to be simultaneously analyzed over several length and time scales.[30] Additionally, to finally propose a generally understandable formation mechanism, concerted and/or cooperative processes have to be separated in time and split into a sequence of individual reaction steps, and chemical reactions not related to nanoparticle formation have to be discarded.

Mechanistic studies can be performed by ex situ as well as by in situ techniques. Most of the studies on nanoparticle formation mechanisms are based on reaction sampling after different times followed by sample preparation and analysis. Such ex situ analysis, also known as indirect sampling, has several limitations. The two most important ones are that indirect sampling is typically time consuming due to rather laborious sample preparation, and that the sample might undergo some changes during the preparation. This problem is especially pronounced for characterization techniques that generally require dried specimens, for example, X-ray powder diffraction or electron microscopy. Drying effects are a particularly serious issue, if nanoparticle formation involves a particle-mediated process. Moreover, indirect sampling not only involves quenching of the reaction solution, hampering the observation of unstable intermediates, but also induces a volume change in the mother liquor, which might affect the chemical equilibrium. Consequently, extreme care has to be taken when conclusions on particle formation mechanisms are drawn from ex situ measurements.

In situ studies, on the other hand, make the individual sample preparation and measurement superfluous, offering a more accurate and time saving approach. Data collection at high frequency, minimization of the perturbation applied to the fragile physico-chemical equilibrium and access to kinetic and dynamic parameters represent additional advantages of in situ investigations. On the other side of the coin, monitoring of dynamic and heterogeneous systems is experimentally challenging. The presence of highly absorbing solvents can suppress the signal of the solid phase. In turn, the solid phase can cause spectral artifacts, baseline shifts or uncontrolled noise, rendering the quantitative analysis of the liquid phase difficult. Side reactions, intermediates present only for short times and/or at low concentrations and finally the lack of theoretical models and dedicated experimental instruments for the study of interfacial reactions in solutions are further obstacles that have to be overcome to establish in situ methods as a generally applicable tool to investigate nanoparticle formation mechanisms. Last, but not least, data analysis and interpretation is often difficult simply due to the immense data volume, but also due to processes, which might occur in parallel, leading to the superimposition of measurement signals.

It is obvious that the various synthesis methods are not equally compatible with in situ techniques. Whereas solution routes are usually easier to combine with in situ probes, gas-phase and solid-state methods are more complex to monitor under reaction conditions. But also among the solution routes there are big differences. Syntheses performed at low temperatures in open vessels are relatively straightforward to study, whereas harsh reaction conditions (high temperature, high pressure, corrosive environments,…) and closed containers cause some troubles. Solutions to these problems are offered by measuring cells that were specifically developed for such reaction systems.[31–33]

The first and most important step on the way to study the formation mechanism of a particular nanomaterial is the careful planning of the experiment, which includes identification of the goals, that is, the information one wants to collect, and selection of the appropriate instruments and experimental conditions. The following questions have to be addressed: Is information on short- or long-range atomic order required? What are the time scales that have to be resolved? What are the optimum concentrations to measure any signals? Is parallel instrumentation required? In addition, it might be necessary to design reactors that are able to accommodate the probes or that are compatible with specialized tools such as synchrotron irradiation. The reactor design has to include considerations about the pressure range, chemical environment and the temperature conditions during nanoparticle growth. Interference between the different probes as well as between the probes and the reaction system itself has to be excluded. Ideally, the

Rupali Deshmukh received her Master's degree in Inorganic Chemistry from the Department of Chemistry, Savitribai Phule Pune University formerly known as University of Pune, India in 2006. After completion of her PhD in Materials Chemistry from Vienna University of Technology, Austria in 2012 she joined the Laboratory for Multifunctional Materials, Department of Materials at ETH Zurich, Switzerland as a postdoctoral researcher. Her research interests include the development of novel solution routes to colloidal nanoparticles, understanding the nanoparticle formation mechanisms, and their applications in various fields.

Markus Niederberger is Chair of the Laboratory for Multifunctional Materials and Full Professor in the Department of Materials at ETH Zurich. He studied chemistry at ETH Zurich, where he also received his PhD. After a postdoctoral stay in the group of Galen Stucky at the University of California at Santa Barbara, he became group leader in the Colloid Department of Markus Antonietti at the Max Planck Institute of Colloids and Interfaces in Potsdam. His research interests are focused on the development of liquid-phase synthesis routes to inorganic nanoparticles, the study of their formation mechanisms, and their assembly and processing into macroscopic materials with tailored properties and functionalities for applications in energy storage and conversion, optics, gas sensing and (photo)catalysis.

monitoring involves noninvasive and orthogonal instrumentation, capable of following all aspects of nanoparticle formation.

In this Review we approach the topic of nonaqueous sol–gel chemistry on different levels and we try to cover several aspects of nanoparticle formation. In the introduction we presented some basic considerations of mechanistic studies on nanoparticle formation. In Section 2, we provide a brief overview of experimental details regarding the synthesis of metal oxide nanoparticles in organic solvents and their basic underlying reaction pathways, leading to the formation of M-OH species and finally to M-*O*-M units. In Section 3, an overview of the different characterization methods used for monitoring nanoparticle formation is presented, including spectroscopic, scattering and microscopy methods. The focus is on the information accessible by a specific method rather than on technical details. Section 4 represents the major part of the review and presents an in-depth discussion of the chemical formation mechanisms observed for different types of metal oxide nanoparticles, categorized according to the reaction systems, that is, precursor and solvent. We start with reactions between metal halides and oxygen donors, followed by reactions between metal alkoxides and alcohols or amines, metal acetylacetonates and alcohols or amines and finally reactions of various precursors with ketones and aldehydes. In Section 5, we discuss a few crystallization studies performed in organic solvents on titania, molybdenum dioxide, tungsten oxide and zinc oxide. Finally, in Section 6 we present selected examples of surface functionalization, which make use of nonaqueous sol–gel concepts. In general, we direct our attention towards publications reporting mechanistic aspects of nanoparticle formation rather than on discussing pure synthesis papers. For a general overview of nonaqueous/nonhydrolytic synthesis routes, the interested reader is referred to dedicated literature.[34–38]

2. Overview of Nonaqueous Sol–Gel Routes to Metal Oxide Nanoparticles and Their Basic Organic Reaction Pathways

In contrast to aqueous sol–gel chemistry, nonaqueous sol–gel routes are performed in organic solvents (not necessarily miscible with water) and work without external addition of water.[34,35,39] However, in situ formed water might still render the process hydrolytic. Therefore, we prefer to use the term "nonaqueous" rather than "nonhydrolytic", although in literature nonaqueous and nonhydrolytic are often used interchangeably. Similar to aqueous systems, nonaqueous sol–gel routes are mainly used for metal oxides, although metal sulfides[40,41] and metal nitrides[42] are also accessible in selected cases.

In a typical nonaqueous sol–gel synthesis, molecular precursors such as metal halides, metal alkoxides, metal acetates or metal acetylacetonates are dissolved in an organic solvent (e.g., alcohols, ketones, amines, hydrocarbons,…) or in a solvent mixture and heated to temperatures between 50 and 250 °C using an oil bath, an autoclave or a microwave reactor (Figure 1, upper part). After the heat treatment, the precipitate (either spontaneously formed or precipitated by adding a nonsolvent) is separated from the reaction liquid by centrifugation, resulting in a powder after drying. The nonaqueous sol–gel routes are applicable to a wide variety of metal oxide nanoparticles, including magnetic, ferroelectric, electrically conducting and doped nanostructures of different sizes and shapes (Figure 1, lower part). Most importantly, the nanoparticles are

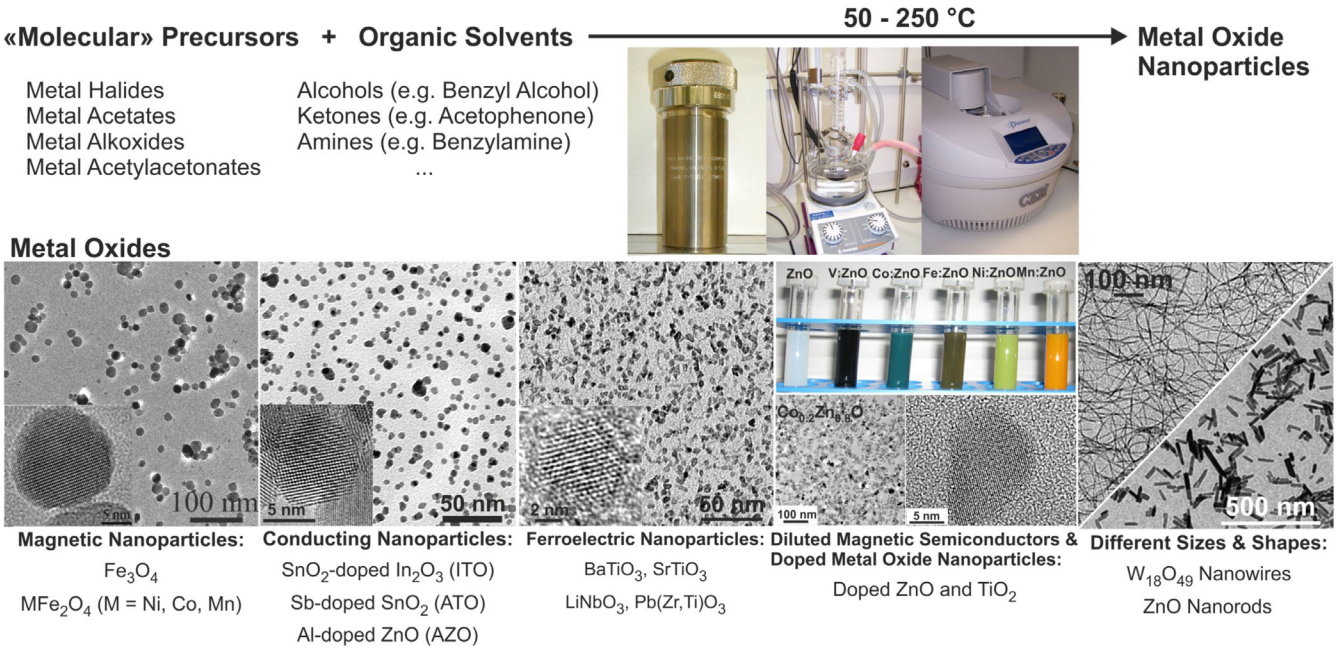

Figure 1. Upper part: Schematic of the nonaqueous sol–gel synthesis approach for metal oxide nanoparticles using autoclave, oil bath or microwave heating. Lower part: Transmission electron microscopy (TEM) images of selected metal oxide nanoparticles and their properties. Reproduced from ref. [43] with permission of Elsevier B.V.

highly crystalline directly after the synthesis. While annealing is not necessary for inducing the crystallization, it is still often applied to remove organic impurities attached to the surface of the nanoparticles.

In comparison to aqueous system, where the water molecules donate the oxygen atom for oxide formation via hydrolysis and condensation, nonaqueous sol–gel processes involve chemical reactions between organic species (e.g., the organic part of the precursor and/or the solvent(s)). Accordingly, the chemistry is determined by the reactivity of the C–O rather than the O–H bond.[44] For the study of formation mechanisms, it is considerably easier to follow the chemical transformation of organic species rather than that of water molecules. Nevertheless, the role of the organic compounds is manifold and can be tremendously complex,[45] including acting as oxygen source, stabilizing agent, surface ligand, reducing/oxidizing agent, or even as constituent of the final product in case of formation of organic-inorganic hybrids.[46–51] As a result, organic species (initially present, but also formed during the reaction) influence crystal size, shape, composition, oxidation state of the metal ions, crystal structure, surface chemistry, and agglomeration/assembly behavior. Having said that, it is obvious that the investigation of nanoparticle formation and crystallization mechanisms in nonaqueous systems has to consider the inorganic and the organic side as well as the organic–inorganic interface.

In aqueous sol–gel processes, hydrolysis and condensation reactions are responsible for the formation of the metal oxides. Hydrolysis of the precursor leads to the formation of M-OH species, which then undergo water or alcohol condensation to form M-*O*-M bonds as basic structural unit of metal oxides. In nonaqueous systems, M-OH and M-*O*-M bonds are also formed, but typically by organic reactions. At this point it is worth to note that most of the principles of nonaqueous/nonhydrolytic sol–gel chemistry have been developed a long time ago for the synthesis of gels.[1] An important aspect in this regard was the progress made in understanding the chemistry of metal alkoxides.[52;53] However, only in the beginning of the 1990ies with the work of Corriu, Vioux and co-workers on monolithic silica, alumina and titania and mixed oxide gels, these methods attracted a broader attention.[54–56]

Nonaqueous sol–gel routes are not necessarily water-free during the whole reaction course. Although the initial reaction mixture might be anhydrous, specific organic reactions are able to produce water in situ (e.g., aldol condensation and esterification reactions), rendering the system in principle hydrolytic. But even in the absence of water, it is possible to have hydroxylation reactions, that is, formation of M-OH species (Scheme 1). Scheme 1 a shows the reaction between metal halides and alcohols. After the coordination of the alcohol to the metal center, elimination of an alkyl halide RX leads to the formation of a M-OH species. Of course, one has to keep in mind that such schematic reaction pathways are idealized and oversimplified. In general, the detailed structure of the M-OH compound is unknown. As a matter of fact, even the structure of the precursor after dissolution in the organic solvent has typically nothing to do anymore with what is written on the purchased bottle, because it immediately reacts with the solvent even at room temperature. Nevertheless, these schemes provide a helpful tool to understand the chemistry, and analysis of the organic products in the final reaction solution often confirms these pathways. The second example (Scheme 1 b) involves a Guerbet-type reaction, in which the alkoxide ligand undergoes a C–C bond formation in β-position to another alcohol (e.g., the solvent) under formation of a metal hydroxide. This pathway is not very common and occurs under alkaline conditions or in the presence of Lewis-acidic metal ions. Examples include the formation of $BaTiO_3$ nanoparticles[57] and yttria nanostructures.[46] Finally, Scheme 1 c displays the formation of M-OH by an aldol condensation between two acetone molecules, which produces water for the hydrolysis of the metal alkoxide and mesityl oxide.

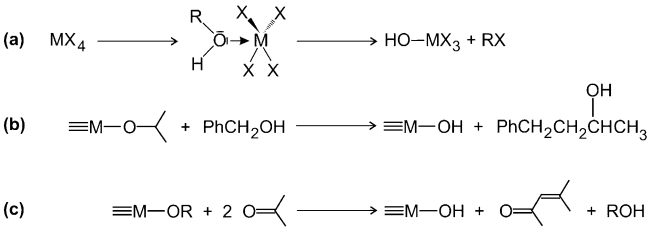

Scheme 1. Overview of nonhydrolytic hydroxylation reactions. (a) Reaction of metal halides with alcohols. (b) Guerbet-type reaction of a metal isopropoxide with benzyl alcohol leading to M-OH and 4-phenyl-2-butanol. (c) Aldol condensation between two acetone molecules. As an example, the metal M is in the oxidation state of 4+. However, the Scheme also applies to any other oxidation state. Scheme reproduced from ref. [34].

Independent of how the M-OH forms, all these species can undergo condensation reactions analogous to aqueous systems, leading to M-*O*-M units.

The formation of M-*O*-M bridges is also possible without the involvement of hydroxyl species, for example, from metal alkoxides, which form upon the reaction of metal halides with alcohols (alcoholysis, Scheme 2 a) or ethers (etherolysis, Scheme 2 b).

Depending on the reaction system, the alkoxy groups subsequently condense into M-*O*-M bonds under release of organic molecules, which define the type of elimination reaction (Scheme 3). Alkyl halide elimination involves the condensation between a metal alkoxide and a metal halide (Scheme 3 a), ester elimination occurs between metal carboxylates and metal alkoxides (Scheme 3 b) and ether elimination is the result

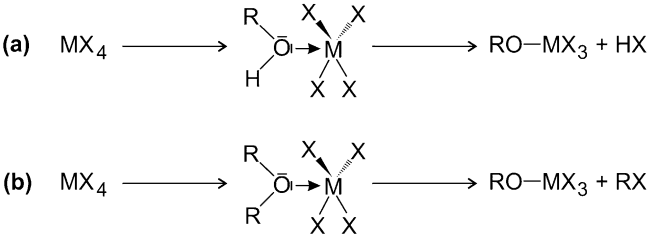

Scheme 2. In situ formation of metal alkoxides by (a) alcoholysis and (b) etherolysis. As an example, the metal M is present in the oxidation state of 4+. Scheme reproduced from ref. [34].

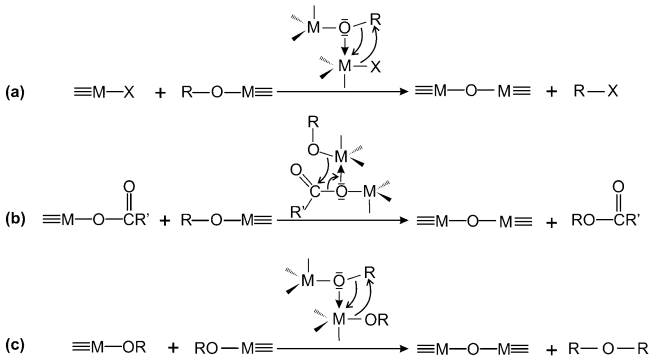

Scheme 3. Condensation mechanisms leading to M-*O*-M units: (a) Alkyl halide elimination, (b) ester elimination, (c) ether elimination. As an example, the metal M is present in the oxidation state of 4+. Scheme reproduced from ref. [34].

of the reaction between two metal alkoxides (Scheme 3 c). Accordingly, determination and quantification of the organic elimination products provide information about possible condensation pathways.

This section just provided a short and schematic overview of the most important and fundamental organic reaction pathways found in nonaqueous sol–gel chemistry. The presented schemes are shown for metal ions in the oxidation state of 4+. However, the same mechanisms apply to metal ions in any other oxidation state. Further mechanistic details can be found in dedicated reviews,[1,36,58] book chapters[34,59] and books.[35] Examples of selected organic reaction pathways observed in the synthesis of specific metal oxide nanoparticles are discussed in Section 4.

3. Overview of Methods To Study Mechanisms

In this section, we will briefly discuss the most common techniques to study nanoparticle formation mechanisms in solution. While these methods have a long tradition in the postsynthetic characterization of powders,[60] meanwhile they also enable in situ investigations. Especially in the field of heterogeneous catalysis, there is tremendous know-how in the in situ characterization of organic and inorganic species as well as their interface.[61] We will put the focus on the type of information, which can be extracted from a specific characterization tool rather than on explaining its working principles (Figure 2). However, we provide additional references for the interested reader. Our discussion is divided into three parts: i) Spectroscopic monitoring involving laboratory as well as synchrotron techniques, ii) diffraction and scattering methods and iii) image-guided microscopy tools. Gas chromatography-mass spectrometry (GC-MS), which does not fit in one of these three categories, is not further discussed in this method section. Nevertheless, it is frequently used to separate, identify and quantify organic compounds as will be shown in Section 4.

3.1 Spectroscopy

Optical spectroscopy has extensively been used for the characterization of the electronic structure of nanoparticles. When

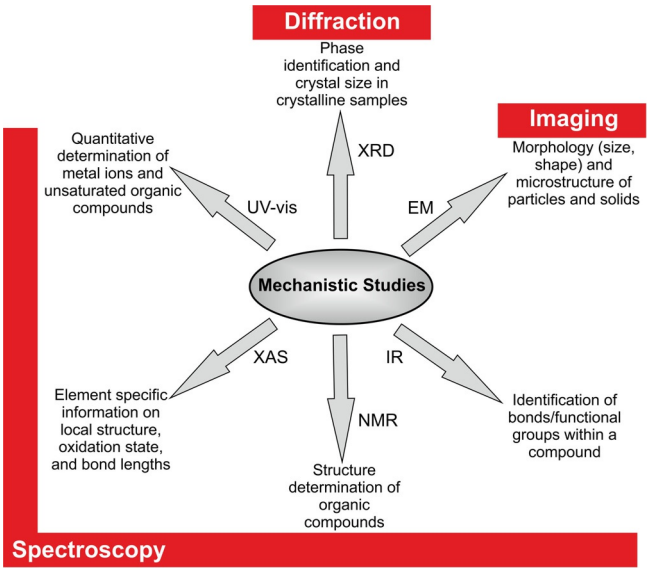

Figure 2. Overview of selected characterization methods together classified into the three categories diffraction, spectroscopy and imaging with the main information gained from these techniques. IR: Infrared spectroscopy; XRD: X-ray diffraction; EM: Electron microscopy; NMR: Nuclear magnetic resonance; XAS: X-ray absorption spectroscopy; UV/Vis: Ultraviolet-visible spectroscopy.

the size of nanoparticles shrinks to just a few nanometers, surface and quantum size effects come into play. Especially in semiconductors these effects lead to a strong dependence of the electrical and optical properties on size.[62] In particular, the band gap energy increases with decreasing particle size, that is, the energy of the band gap absorption and that of the emission increase and become sensitive to the size and shape of the particles.[63] In addition to the shift in band gap energy as a function of primary particle size, one could also expect to see discrete features in the spectra. In metal oxides this is however not the case. The influence of the nanostructure in optical spectroscopy data is mostly restricted to the absorption onset energy, because the particle size distribution induces broadening of the spectrum and limits the study of the shape of the optical absorption spectrum.[60] Nevertheless, it is easily possible to extract information about the primary particle size from simple UV/Vis measurements. Especially ZnO nanocrystals show a pronounced shift of the band gap and consequently of the absorption edge with size, and several studies took advantage of this effect to monitor nucleation and growth of ZnO nanoparticles in solution.[64–67] As a matter of fact, the formation mechanisms of ZnO nanoparticles have been extensively studied.[68] Further insight into the characterization of heterogeneous catalysts by UV/Vis spectroscopy with special emphasis on transition metal ion containing catalysts can be found here.[69]

Infrared spectroscopy (IR) is a widely used technique to characterize samples in the liquid, solid, or gas state. IR spectra represent fingerprints specific for a molecule or a material, and thus enable their identification in a sample. Moreover, the vibrational spectrum is sensitive to the environment of the mol-

ecule, and therefore shifts of absorption bands are indications for changing interactions such as formation or cleavage of bonds, which is perfect for reaction monitoring. Although IR is a well-established method, it brings along a few issues that have to be considered during in situ studies in liquid phase. The main limitation is the strong IR absorption by the reaction mixture comprising reactants, products and in most cases a solvent.[70] The problem can be overcome by using the ATR (Attenuated Total Reflection) technique. In this case, only the sample close to the IR probe is measured (typically within the range of a few μm), minimizing the contribution from the liquid. Another limitation is the spectral overlap, if several species contribute to the IR spectrum. In this case, the interpretation of the different bands and their assignment to specific compounds is difficult. A possible solution for this problem is the implementation of multivariate data analysis tools, which offer a chemometric approach to resolve multiple component responses in unknown mixtures.[71,72] ATR-FTIR (Attenuated Total Reflection-Fourier Transform Infrared Spectroscopy) has extensively been used to study for example, heterogeneous catalysis in water[70] or solid/liquid interfaces.[73–75] In the field of nanoparticle research, IR is mainly used for the characterization of surface bound organic species. Inspired by the results obtained in the field of catalysis, in situ ATR-FTIR became also attractive for the study of nanoparticle formation mechanisms by following the organic compounds and their interaction with the growing nanoparticles. Typically, only completely dissolved species are visible in the IR spectra.[76] However, if the nanoparticles are in close contact with the IR probe, for example, if they grow on the probe, then it is possible to get information about their surface functionalization.[77] An instructive example was reported by Garnweitner and Grote, who studied the molecular kinetics and particle formation of water-dispersible titania nanocrystals from $TiCl_4$ in a benzyl alcohol-ethanol mixture by in situ ATR-FTIR.[76] The ATR probe was directly immersed into the reaction mixture. In spite of the fact that the IR spectra were dominated by the solvent benzyl alcohol, it was possible to evaluate and identify the organic compounds formed or consumed during the particle formation process. The bands assigned to benzyl chloride and benzyl ether increased with reaction time, indicating that alkyl halide and ether elimination were the main organic reactions involved in titania formation. The IR data also revealed that these two organic reactions occurred independently and possessed different kinetics. ^{13}C and ^{1}H NMR spectroscopy investigations confirmed the IR results and additionally provided information about the interaction of the solvent with the particle surface. The formation of the titania nanoparticles was monitored by ex situ transmission electron microscopy (TEM) and dynamic light scattering (DLS) measurements.

Raman spectroscopy is a powerful tool to analyze structural/morphological properties of solid oxides, providing information about the existence of lattice defects and oxygen vacancies. However, for mechanistic studies in liquid phase and especially in organic solvents Raman is less suitable due to the intrinsically low sensitivity, resulting in extremely weak signals and due to the strong absorption of the organic solvents.

More suitable for in situ studies is X-ray absorption spectroscopy (XAS), typically divided into the EXAFS (extended X-ray absorption fine structure) and the XANES (X-ray absorption near edge structure) region. Such measurements provide detailed information about the chemical environment of a specific element, but it requires synchrotron radiation and elaborate data analysis.[78] Nevertheless, the method is extremely powerful for the study of nanoparticle formation mechanisms, especially when the reaction system is and behaves complex (e.g. the initial reaction mixture consists of many chemicals; the reaction process is characterized by chemical and structural inhomogeneity; the metal ions undergo redox reactions;…).[29] The main advantage of XAS is that it makes it possible to look selectively at a specific element in solution (even when highly diluted) with high temporal resolution up to milliseconds to probe the local atomic environment including bond distances, coordination number and the type of surrounding atoms.[29,78] XAS techniques are often used in conjunction with X-ray diffraction, thus extending the accessible length scale from the atomic site to systems undergoing crystallization.[79] An instructive example, even though the synthesis was not performed in an organic solvent, was presented by Patzke et al., who reported an in situ study on the hydrothermal formation of MoO_3 nanofibers by a combination of XANES/EXAFS and energy dispersive XRD techniques.[80] These complementary tools enabled the monitoring of the long- as well as the short-range order, which was important to provide a full picture of nanoparticle formation from the nucleation to growth and precipitation. The autoclave cell was designed in a way that it allowed the observation of both the solid and the liquid phase by EXAFS. Local observation of the bulk liquid and the solid–liquid interface gave information about the dissolution of the precursor and the crystallization of the product. The same approach can also be applied to metal oxide nanoparticles synthesized in organic solvents. Using a similar cell, the formation of MoO_2 nanoparticles from MoO_2Cl_2 in a mixture of benzyl alcohol and acetophenone was studied.[81] XAS allowed monitoring of the reduction of Mo^{6+} to Mo^{4+}, while the cell design with two X-ray permeable windows at the bottom and in the middle of the cell made it possible to follow the precipitation process. As a result, a relation between precursor reduction and nucleation of MoO_2 could be established. If the complexity of this system is increased by adding nickel acetate to the initial reaction mixture to produce Ni-doped MoO_2, then XAS measurements clearly indicated that already the nuclei had the same composition like the final nanoparticles (contrary to the hypothesis that first the pure host material nucleates and the dopant is incorporated into the lattice only during the growth process). Other systems were found to be unexpectedly complex. Even though they just consisted of a precursor and a solvent, redox reactions occurring in parallel (rather than consecutively) resulting in different oxidation states of the metal species significantly complicated in situ analyses. An example in this direction is the formation of cobalt and cobalt oxide nanoparticles in benzyl alcohol.[33] Starting from Co^{2+}, these ions were simultaneously oxidized to Co^{3+} and reduced to Co^0. The partial oxidation was followed by a rapid formation of Co_3O_4

nanoparticles and its consecutive solid-state reduction to CoO. In parallel, metallic Co nanoparticles begun to grow directly from the reduced species. The XAS data was evaluated by MCR-ALS analysis. This example shows that XAS can be used to determine the interdependence between nanoparticles with varying compositions and between ions with different oxidation states in solution.[29]

Nuclear magnetic resonance (NMR) spectroscopy is the most widely used method for the identification and structure determination of organic molecules in solution by typically probing the chemical environment of ^{1}H and ^{13}C. However, the method is not restricted to liquids, but can also be applied to solids, which makes it a useful tool for in situ catalysis and crystallization studies.[82] For example, Harris et al. proposed a method to follow the crystallization of organic molecules from liquid phase either under complete exclusion of any contributions from the liquid phase, just selectively measuring the solid particles,[83] or by simultaneously following the evolution of both the liquid and the solid phases.[84] Solid state NMR spectroscopy is not a very sensitive method, when compared with other spectroscopic techniques.[82] However, the development of special techniques such as magic-angle spinning (MAS) or cross polarization MAS (CP-MAS) together with sample cells suitable for experiments at elevated temperatures and pressures considerably improved its potential for in situ studies.[85] While the observation of organic molecules is straightforward, inorganic solids are only accessible if they contain NMR active nuclei such as ^{29}Si, ^{27}Al or ^{31}P. But even in such a case, the acquisition of a spectrum typically requires several minutes, and therefore NMR has rarely been used to monitor the nucleation and growth of metal oxides. Nevertheless, solution NMR is still able to make great contributions to metal oxide nanoparticle research by focusing on the role of organic species either as condensation products during nanoparticle formation and/or as surface-active species. As discussed in the second part of Section 2, the formation of M-*O*-M bonds goes along with organic elimination reactions. To find out, which organic pathway is taken during the formation of a specific metal oxide, one can simply analyze the organic compounds in the final reaction mixture by ex situ ^{1}H and ^{13}C NMR. By retro-synthetical analysis it is then possible to correlate the processes leading to these organic compounds to the chemical formation mechanisms of the oxide nanoparticles.[44] A simple example is the synthesis of HfO_2 nanoparticles from hafnium(IV) ethoxide and benzyl alcohol. NMR characterization of the final reaction solution proved the presence of different types of organic ethers, which clearly pointed to an ether elimination process (Scheme 3 c).[86] The second important contribution of NMR techniques is in the area of surface characterization of colloidal nanocrystals.[87] In many synthesis procedures, surfactants and organic additives are used to control nucleation and growth of nanocrystals, to prevent their agglomeration, and to functionalize their surface. As surface-bound organic species strongly affect the physical and chemical properties of nanoparticles, it is of course essential to have a clear picture about the surface chemistry. Garnweitner et al. revealed a different stabilization mechanism for indium tin oxide and zirconia nanoparticles in the presence of weakly and strongly binding ligands by solution ^{1}H and ^{13}C NMR.[88] Another interesting feature of NMR measurements is the possibility to distinguish between free species in solution and species interacting with or bound to the nanocrystals.[87] In addition to the identification of the organic species, it is even possible to quantify the bound and free ligands.[87] Another interesting feature is the direct observation of ligand exchange reactions. Such exchanges are important to tune the dispersibility behavior of the nanocrystals in solvents with different polarity, or simply to perform chemical reactions on the surface of the nanoparticles. Regarding the latter, a fascinating example was reported by De Roo et al., who reported a catalytic ester formation between oleic acid molecules bound to the surface of hafnium dioxide nanoparticles and ethanol (Figure 3).[89] NMR spectra acquired at different reaction times showed that initially the ester concentration increased linearly with time, while the ethanol concentration decreased and the surface-bound oleic acid remained constant. All adsorption sites set free by the ester formation were obviously replenished by freshly added oleic acid, maintaining the surface composition of the hafnia nanoparticles.

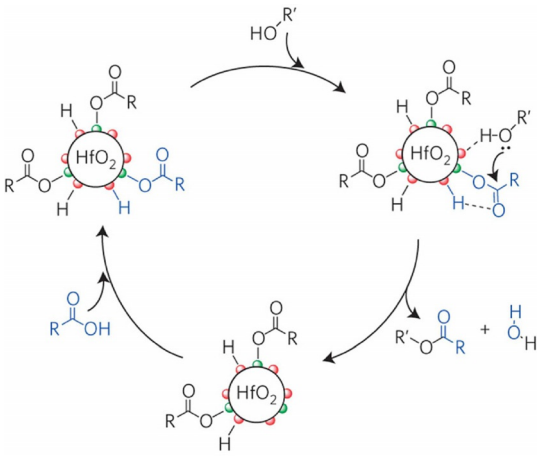

Figure 3. Schematic of the esterification reaction between surface-bound carboxylic acids and added alcohol catalyzed by hafnia nanoparticles. Figure reproduced from ref. [89] with permission of Nature Publishing Group.

3.2 Scattering Methods

In situ X-ray diffraction (XRD) techniques have mainly been applied in the investigation of solid state transformations.[90] However, with the development of suitable reaction cells, also the study of crystallization processes became easier and more popular.[33,79,91,92] X-ray diffraction provides information about the crystallization kinetics, evolution and composition of the crystalline phase(s), phase transformations, crystal size and anisotropy. Structures without long-range order can be probed by total X-ray scattering combined with atomic pair distribution function. Especially information on precrystalline species and processes such as molecular transformations, discrete clusters or small nanoparticles are accessible, even under supercritical conditions.[93–97] Most of the early in situ X-ray diffraction studies were focused on the crystallization of zeolites[98] and other

microporous[99] or mesoporous[100] materials grown under hydrothermal conditions. In the case of nanoparticle synthesis the focus is directed towards the study of nucleation and growth, because these processes determine the size, the size distribution and the shape of the nanoparticles, and all these factors are fundamental for their properties. Due to the fact that most syntheses deal with the preparation of crystalline nanoparticles, powder diffraction techniques represent a powerful tool to monitor the course of particle formation in situ under real conditions. However, as most of the nanoparticle syntheses are not performed under ambient conditions, dedicated cells have to be developed, fulfilling the following requirements:[90] i) The intensity of the radiation used must be high enough to produce a good signal under reaction conditions, ii) the geometry of the cell design has to allow unhindered penetration of the X-ray beam, iii) the reaction mixture in the cell has to be brought to the appropriate reaction conditions, that is, heated or cooled, and the cell has to withstand these reaction conditions, and iv) the rates of the processes to be monitored have to be matched with the data acquisition speed, so that the desired information is indeed accessible from the data. In situ X-ray diffraction experiments can be performed using either laboratory X-ray diffractometers or synchrotron X-ray sources. However, examples on mechanistic studies on nanoparticle growth in liquid medium using laboratory diffractometers are scarce because of the poor quality of the data due to strong absorption of the X-ray beam by the reaction chamber and the synthesis solution. In comparison to typical laboratory X-ray diffraction, synchrotron radiation offers a much higher brightness, which makes it possible to collect high-resolution data in very short times, but also to minimize absorption effects from the sample holder and the reaction mixture. Both advantages are important, because one can perform the experiments in larger cells, and the shortened data accumulation time allows to follow faster chemical reactions.

Such in situ XRD studies are not only interesting from a fundamental mechanistic point of view, but also with respect to a rational tuning of the materials composition after the synthesis (Figure 4). In the case of the reaction of copper(II) acetylacetonate with benzyl alcohol,[101] it was shown by in situ synchrotron X-ray diffraction that the process involved the transformation of Cu^{II} ions into solid Cu_2O, followed by solid state reduction of the oxide into metallic copper.[102] Regarding post-synthetic modification of the composition, in situ laboratory XRD study revealed details about the oxidation behavior of the copper, enabling the controlled transformation of the metallic copper compound into single-phase CuO or into heterostructured Cu_2O/Cu through thermal treatment.[102] Heterostructures find widespread applications in photovoltaics, photocatalysis, batteries or in gas sensors.

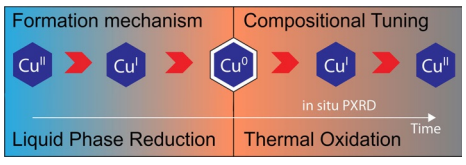

Figure 4. Overview of the mechanism of metallic copper formation from copper(II) acetylacetonate and its transformation into CuO and Cu_2O/Cu by thermal treatment. Adapted from ref. [102].

In comparison to X-ray diffraction, which mainly deals with the atomic structure of crystals, small-angle X-ray scattering (SAXS) probes relatively large structures such as polymers, nanoparticles, colloids, and biological macromolecules.[103,104] Nevertheless, SAXS covers a broad range of length scales from a few angstroms to several micrometers,[103] which makes it a perfect tool to study nucleation and growth. SAXS records electron density differences in the sample and therefore it is also sensitive to amorphous materials. The measurements, especially under in situ conditions in liquid samples, are typically performed with synchrotron irradiation. The information obtained includes particle size, size distribution, shape, internal structure and concentration, but also information about the dynamics of the particles (e.g., agglomeration or gelation) is accessible. It is important to mention that while XRD yields the crystal size, SAXS measures the particle size, which is different in case of polycrystalline particles. But in spite of all these attractive features of SAXS, the data is not always straightforward to interpret due to its relatively featureless patterns (compared with crystal diffraction data) and its high sensitivity to the experimental technique and sample quality.[105] Common problems are polydispersity of the sample, non-spherical particle shapes and poor background subtractions. Therefore, SAXS data analysis is typically supported by electron microscopy investigations, giving information on particle size distribution and particle shape. But even in such a case, data fitting still often remains a time-consuming task.

One of the very few SAXS studies on non-spherical metal oxide nanoparticles obtained by a nonaqueous sol–gel process is dedicated to the crystallization mechanism of tungstite nanoplatelets.[106] These particles, synthesized from WCl_6 and benzyl alcohol, formed by a complicated crystallization process involving nucleation of spherical particles, their assembly into rod-like structures and finally internal rearrangement into crystallographically oriented stacks of platelets. The SAXS patterns could be fitted to such a particle-mediated growth process, although the SAXS curves were relatively smooth without clearly assignable structural features due to the polydispersity of the scattering particles. But also here, time-dependent ex situ transmission electron microscopy investigations helped to interpret the complex SAXS data.

3.3 Microscopy

Transmission electron microscopy (TEM) is one of the most powerful tools to directly image nanoparticles to get information about their size and shape, but also about formation of agglomerates or superstructures such as superlattices or mesocrystals. In the high-resolution (HR) and diffraction mode, information on crystal symmetry, crystallographic phase, and crystal orientation is accessible, enabling determination of crystal growth directions and crystallographic orientation of nanocrystals within an agglomerate or ensemble. Accordingly, TEM is able to provide a complete picture of the morphological and

structural features of nanoparticles, however, with the disadvantage that the information is extracted only from a small part of the sample. The limited statistics is probably the main limitation of TEM methods. But TEM is by far not restricted to imaging. Combined with energy dispersive X-ray spectroscopy (EDS) and electron energy-loss spectroscopy (EELS) also the chemical and electronic structure of nanoparticles can be measured, providing local information on the elemental composition, elemental distribution or valence state. In the scanning mode, in which the finely focused electron beam scans over the sample, the resolution for these spectroscopy tools reached the atomic level. An example in this direction reported the use of EELS imaging in a scanning transmission electron microscope (STEM) combined with multivariate statistical analysis to map the distribution of Ba dopant atoms in $SrTiO_3$ nanoparticles.[107] New developments such as electron microscopy of specimens in liquid[108] or electron tomography, enabling a three-dimensional picture of nano objects, or the availability of in situ cells continuously expand the repertoire and make electron microscopy techniques even more attractive.[109–111] Considering that electron microscopy is an ultra-high vacuum technique, the implementation of dedicated cells for directly probing the dynamics of gas–solid, liquid–solid and liquid reactions at the atomic scale is amazing. It is obvious that for the study of nucleation and growth of nanoparticles in solution such a tool opens up completely new possibilities. In this case, the low statistics of TEM is an advantage, because it enables monitoring of a single event, revealing information, which is hidden by methods producing a signal averaged over the whole sample. In their pioneering work, Zheng et al. made use of the electron beam to reduce Pt cations and thus trigger their nucleation.[112] The study revealed two growth scenarios of the nanoparticles, either by classical monomer attachment or by random coalescence with subsequent intraparticle reorganization. Meanwhile, the liquid cell has been improved to increase the resolution,[113] and other systems and processes have been monitored like the oriented attachment of iron oxyhydroxide nanoparticles[114] or the growth of Pt_3Fe nanorods.[115] Clearly, the fascination of TEM is not only rooted in its scientific merit, but also in the fact that it is always nice to "see" things happening with our eyes. More details on recent advances in in situ TEM and a historical outline can be found in the review of Chen et al.[116]

At this point we finish our summary on in situ methods. A last reference is made to the review article of Pienack and Bensch, who comprehensively summarized the different in situ methods available for the study of the early stages of crystallization of solids.[85]

4. Chemical Formation Mechanisms

In nonaqueous sol–gel synthesis, the selection of the appropriate precursors and solvents defines the characteristics of the resulting nanocrystals including structure, composition, size, shape, surface ligands, and crystallinity,[38,44,117,118] and it also determines the rate of the reaction, nucleation, growth and surface chemistry of nanocrystals.[15,119,120] Another important aspect to be considered is that the use of organic surfactants or surface-active ligands during synthesis may introduce completely new effects.[121]

In the following section, we provide the reader with an understanding of the organic reaction mechanisms behind nanoparticle formation in a specific precursor-solvent mixture. In addition to metal oxides, selected reaction mechanisms responsible for the formation of metal and metal nitride nanoparticles are also briefly discussed. The section is structured according to the different precursor–solvent systems used in nonaqueous sol–gel processes. While the very basic and fundamental mechanisms were introduced in Section 2, we now focus on specific examples reported in the literature for these different mechanisms. It is important to mention that most of the schemes represent a simplified molecular picture. Often the involved species are not monomolecular, but polynuclear metal complexes or clusters, whose structures are typically unknown. The transient nature of intermediate species makes their characterization extremely challenging. For example, a recent study by Garnweitner and co-workers showed the presence of defined oligomeric coordination complexes during the growth of anatase nanoparticles from titanium isopropoxide in benzyl alcohol.[122] Using various NMR spectroscopy techniques and single crystal structure determination they were able to determine several intermediate species including a dimeric titanium benzyloxide $[Ti(OBn)_4(HOBn)]_2$ with BnOH representing benzyl alcohol. While this compound formed rather early in the synthesis, it was not recognized as the monomeric species for particle formation, but reacted to $[Ti_{16}O_{16}](OBn)_{32}$, which transformed into anatase.[122]

In spite of these findings about the complex nature of the intermediates, simplified schemes are still useful to explain many experimental observations and they provide valuable insight into the chemical pathways during the transformation of the precursors to the final nanoparticles.

4.1 Reaction between metal halides and oxygen donors

4.1.1 Reactions between metal halides and metal alkoxides

A broad variety and the low cost of metal halides represent two obvious reasons for their widespread use as a precursor for nanoparticle synthesis. The direct condensation between metal halides (usually chlorides) and metal alkoxides with the elimination of alkyl halide (Scheme 3a) provides a nonaqueous route for the synthesis of metal oxide gels[123,124] and nanoparticles.[125,126] The mechanism of condensation of metal chloride and metal alkoxide involves the coordination of the oxygen of the alkoxy group to the metal bearing chloro substituent, followed by cleavage of the O–R bond with elimination of alkyl halide and formation of M-*O*-M linkages (Scheme 3a). In 1999, Colvin and co-workers reported the synthesis of crystalline titania nanoparticles based on alkyl halide elimination between TiX_4 and $Ti(OR)_4$ in the presence of trioctylphosphine oxide as surfactant at 300 °C. Based on the fact that the reaction rate dramatically increased with greater branching of R, with nearly no influence from the nature of the halide, indicated that the nucleophilic attack of the halide at the alkoxide carbon

proceeded by an S_N1 mechanism.[125] Joo et al. reported the synthesis of 4 nm sized ZrO_2 nanoparticles using a surfactant assisted nonhydrolytic reaction between Zr(IV) isopropoxide and $ZrCl_4$ at 340 °C. The formation of isopropyl chloride and propylene (the product of dehydrochlorination of isopropyl chloride) as a byproduct of the reaction clearly confirmed the alkyl halide elimination reaction pathway.[127] Brus and co-workers reported the nonhydrolytic synthesis of HfO_2 and $Hf_xZr_{1-x}O_2$ nanocrystals via condensation of hafnium isopropoxide and hafnium halides and cross condensation of Hf/Zr(O*i*Pr)$_4$ and Zr/$HfCl_4$, respectively.[128]

In addition to nanoparticles, the nonhydrolytic reaction between metal halides and metal alkoxides allows atomic layer deposition (ALD) of metal oxide thin films.[129,130] Brei et al. confirmed the elimination of ethyl chloride between $TiCl_4$ and $Si(OEt)_4$ by mass spectrometry during the ALD growth of titanium silicate.[131] Rahtu et al. found that the principle reaction responsible for the ALD of $Zr_xTi_yO_z$ is the release of 2-chloropropane between $ZrCl_4$ and titanium isopropoxide.[132] Anderson et al. alternatively reacted $TiCl_4$ and titanium tetraisopropoxide on the surface and monitored the TiO_2 growth by in situ FTIR spectroscopy and studied the byproducts by quadrupole mass spectrometry. At temperatures between 125 and 225 °C, the reaction of $TiCl_4$ with surface isopropoxide species resulted in the formation of Ti–O bonds and 2-chloropropane via alkyl halide elimination reaction. At temperatures between 250 and 300 °C, the surface isopropoxide species were converted to hydroxyl species via the β-hydride elimination reaction. The authors detected propene, which is produced by the β-hydride elimination of the isopropoxide species.[133]

4.1.2 Reactions between metal halides and alcohols or ethers

The reactions between metal halides and alcohols are among the most widely used methods for the nonaqueous synthesis of metal oxide nanoparticles.[134] An alternative route involves the reaction between metal chlorides and organic ethers.[126,135–137] Interestingly, during the alcoholysis or the etherolysis of metal halides, metal alkoxides are generated in situ under elimination of HX[138] or an alkyl halide[123] (Scheme 2). The condensation reaction of these metal alkoxides with unsolvolyzed metal halides under alkyl halide elimination leads then to a M-*O*-M framework (Scheme 3 a). Another possibility to form M-*O*-M bonds is the reaction between two in situ formed metal alkoxides with the elimination of an ether (Scheme 3 c). It is important to note that the HX generated from the alcoholysis of metal halides can catalyze the condensation between two alcohols to produce the ether and H_2O (see also Scheme 4, Equation (6)).[138]

Based on IR and NMR analyses of the reaction byproducts, Pokhrel et al. proposed the alkyl halide and ether elimination mechanism for the formation of WO_3 nanomaterials from WCl_6 and benzyl alcohol using the bioligand deferoxamine mesylate as structure-directing agent.[139] The partial exchange of chloride ions of WCl_6 by benzyl alcohol resulted in the formation of a tungsten alkoxide and HCl. The condensation between WCl_6 and tungsten alkoxide yielded W-*O*-W bonds under elimination

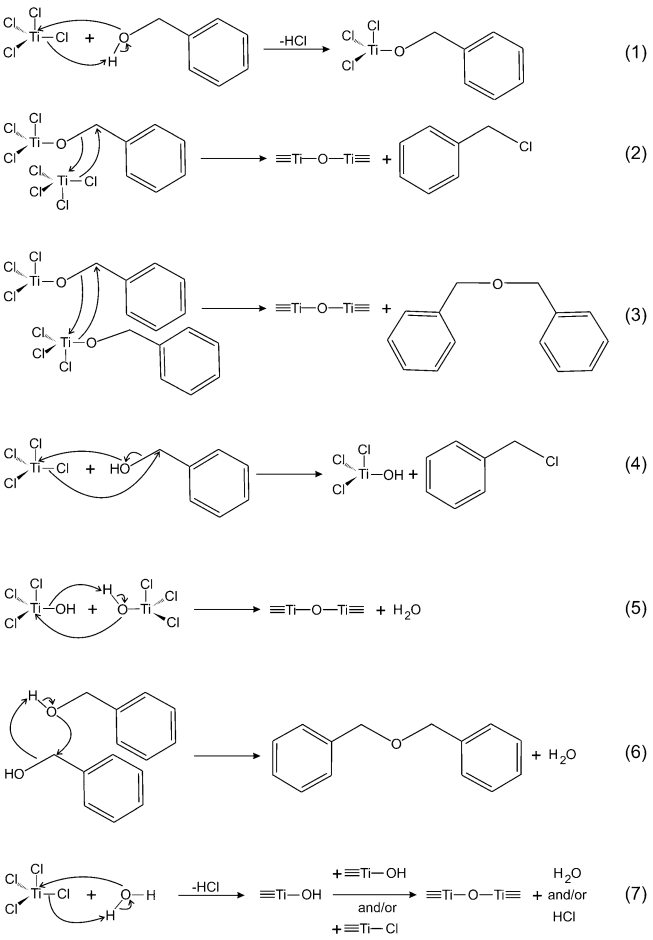

Scheme 4. Possible reactions in the $TiCl_4$-benzyl alcohol system: (1) Ligand-exchange reaction under HCl elimination, (2) Ti-*O*-Ti bond formation under benzyl chloride elimination, (3) Ti-*O*-Ti bond formation under dibenzyl ether elimination, (4) alcoholysis under benzyl chloride elimination, (5) condensation reaction between two titanium hydroxyl species, (6) condensation of two benzyl alcohol molecules into dibenzyl ether, (7) hydrolysis and condensation of $TiCl_4$ either by water or HCl elimination.

of benzyl chloride. Another way to W-*O*-W bonds involved the condensation between two tungsten alkoxides via dibenzyl ether elimination.

Tian et al. proposed a benzyl chloride and dibenzyl ether elimination pathway for the nonaqueous synthesis of reduced graphene oxide-BiOCl hybrid materials from $BiCl_3$ and benzyl alcohol.[140] Garnweitner et al. reported that alkyl halide and ether elimination mechanisms proceeded concurrently during the formation of TiO_2 nanoparticles in a benzyl alcohol-ethanol system, following first-order kinetics. The addition of ethanol to $TiCl_4$ instantly resulted in a ligand exchange reaction to form $TiCl_2(OEt)_2$, which then reacted with benzyl alcohol to form TiO_2 under elimination of benzyl chloride and dibenzyl ether.[76] The same group also investigated the reaction mechanism of TiO_2 formation from $TiCl_4$ and a benzyl alcohol-ethanol mixture in the presence of organic ligands and they did not observe any pronounced effects of the added ligands on the mechanisms and kinetics of the organic condensation reactions.[141]

Scheme 4 summarizes all the possible reactions in the system $TiCl_4$-benzyl alcohol. Equation (1) describes a ligand exchange reaction, where a benzyl alcohol molecule replaces a chloride under HCl elimination. This intermediate chlorobenzyl alcoholate complex can react either with an unsolvolyzed precursor to a Ti-*O*-Ti bridge under benzyl chloride elimination (Equation (2)) or with a solvolyzed precursor under dibenzyl ether elimination (Equation (3)). If the precursor reacts with benzyl alcohol under benzyl chloride elimination, then a hydroxyl species is formed (Equation (4)), which can undergo regular water condensation (Equation (5)). Finally, condensation between two benzyl alcohol molecules (Equation (6)) represents another route to the in situ generation of water, which can hydrolyze and condense the precursor (Equation (7)). This Scheme shows, on the one hand, that even a simple system just consisting of a halide precursor and an alcohol has many possibilities to form a metal-oxygen-metal bond, and, on the other hand, that it is not easy to distinguish between completely water-free processes and hydrolytic processes involving in situ generated water.

Tertiary and benzylic alcohols, due to their ability to form stable carbocations, prefer to eliminate alkyl halides, leading to metal hydroxyl species by a so-called nonhydrolytic hydroxylation reaction (Scheme 1 a), rather than forming metal alkoxides under elimination of hydrogen halides (Scheme 2 a).[142–144] The reaction of primary and secondary alcohols with $SiCl_4$ gave tetraalkoxysilanes, while the same reaction with tertiary and benzylic alcohols yielded silica and the corresponding alkyl halides.[54,145] Li and co-workers highlighted the synthesis of TiO_2, Fe_2O_3 and ZnO from the corresponding metal chlorides and benzyl alcohol from the perspective of a S_N1 reaction mechanism.[143] The carbon-oxygen bond in benzyl alcohol was easily broken, because the formation of a benzyl carbocation is favored due to the possibility to effectively distribute the charge onto the benzyl group via p–π conjugation. The benzyl carbocation then underwent nucleophilic substitution with chloride ions to form benzyl chloride and a metal hydroxide, which further reacted to the metal oxide. The authors also mentioned an interesting side reaction at high temperatures, namely the polymerization of benzyl alcohol in the presence of metal chlorides. A similar polymerization reaction was also observed during the synthesis of magnetite nanoparticles from iron chloride in benzyl alcohol.[144] The authors proposed an analogous S_N1 reaction pathway leading to the formation of Fe-OH species and benzyl chloride, which underwent a polymerization reaction with other benzyl alcohol or benzyl chloride molecules via Friedel–Crafts reaction.[144] The polymerization of benzyl alcohol will be discussed in more details in Section 4.2.1.

Li and co-workers reported an E1 reaction induced synthesis of TiO_2, FeOOH, Fe_2O_3 and SnO_2 nanostructures by reacting the respective metal chloride precursors with *tert*-amyl alcohol. Also here, the high stability of tertiary carbocations and the strong interaction of Lewis acidic metal chlorides with hydroxyl groups resulted in the easy dissociation of the carbon-oxygen bond in *tert*-amyl alcohol. The intermediate carbocation eliminated a proton and became an alkene following the E1 reaction mechanism. However, sometimes a S_N1 reaction can also occur due to nucleophilic substitution of chloride ions for hydroxyl groups.[142]

Zhu et al. developed a nonhydrolytic approach to anatase TiO_2 nanocrystals with dominant {001} facets by solvothermal reaction of TiF_4 in *tert*-butanol. The proposed mechanism is based on the alcoholysis of TiF_4 followed by alkyl halide elimination via formation of a stable carbocation. The elimination of *tert*-butyl fluoride was confirmed by ^{19}F-NMR analysis. The authors also demonstrated that by using different alcohols or by changing the ratio between two alcohols, both the percentage of exposed {001} facets and the particle size could be adjusted.[146] A microwave assisted reaction between $TiCl_4$ and polyethylene glycol was reported for the synthesis of surface-stabilized titanium dioxide nanoparticles. High-performance liquid chromatography-mass spectrometry and FTIR analysis pointed to both an alkyl halide elimination via S_N1 and alcoholysis with elimination of HCl via S_N2.[147] Olliges-Stadler et al. studied the organic and inorganic species involved in the formation of tungstite nanoparticles from WCl_6 and benzyl alcohol by time-dependent gas chromatography, X-ray diffraction as well as by time-resolved in situ X-ray absorption near edge structure (XANES) and extended X-ray absorption fine structure (EXAFS).[148] The formation of benzyl chloride and dibenzyl ether at a very early stage of the reaction indicated two ligand-exchange reactions. The rapid increase in concentration of benzyl chloride was a result of the direct substitution of chlorine with hydroxyl groups, while the generation of dibenzyl ether stemmed from the substitution of chloride by a benzyl alcoholate group, followed by dibenzyl ether elimination. EXAFS analysis revealed WCl_4 and $WOCl_4$ as intermediates. Obviously, addition of WCl_6 to benzyl alcohol led to fast chloride substitution and partial reduction, followed by the formation of intermediates with W=O double bonds and finally by the growth of the W-*O*-W network of the tungstite structure. Ohayon and Gedanken used ultrasonic irradiation for the synthesis of crystalline TiO_2, WO_3 and V_2O_5 nanostructures via the reaction of the respective transition metal chlorides with benzyl alcohol. The elimination of benzyl chloride was confirmed by NMR analysis of the final reaction solution. The formation mechanism involved both, a hydroxylation process with an alkyl halide elimination, and a ligand exchange reaction with the elimination of hydrogen halide.[149]

4.2. Reactions between metal alkoxides and alcohols

4.2.1 Ether elimination

Ether elimination between metal alkoxides leads to the formation of M-*O*-M bonds as shown in Scheme 3 c. In 1956, Bradley et al. discovered the reaction of ether elimination during their investigations on the transformation of metal alkoxides into oxoalkoxides.[150,151] Turova et al. reported the release of diethyl ether from an alcohol solution containing $MoO(OEt)_4$ in the presence of pronouncedly basic lithium and sodium ethoxides, resulting in the precipitation of Li_2MoO_4 and Na_2MoO_4.[152] Kessler et al. found that the molybdenum alkoxides $MoO(OCH_3)_4$ and $MoO(OCH_2CH_3)_4$ reacted rapidly with aldehydes and ketones, transforming the former into colloidal oxidic

compounds and the latter into acetals and ketals, respectively.[153] Pazik et al. reported the nonhydrolytic sol–gel synthesis of crystalline $BaTiO_3$ nanoparticles by means of an ether elimination reaction.[154] Inoue and co-workers synthesized microcrystalline tetragonal zirconia by thermal treatment of zirconium *n*-propoxide in glycol at 300 °C. In a first step, 1,4-butanediol binds to the zirconium center, forming a zirconium glycoxide intermediate, which in a second step undergoes an intramolecular condensation reaction to eliminate tetrahydrofuran, a cyclic ether.[155]

In recent years, the reaction between metal alkoxides and alcohols involving ether elimination has been widely applied for the nonhydrolytic synthesis of crystalline metal oxide nanoparticles. Benzyl alcohol favors the ether elimination reaction during solvothermal treatment with early transition metal alkoxides.[86,156,157] Pinna et al. reported an ether elimination reaction during the solvothermal synthesis of HfO_2 nanoparticles from hafnium(IV) ethoxide and benzyl alcohol (Scheme 5a).[86]

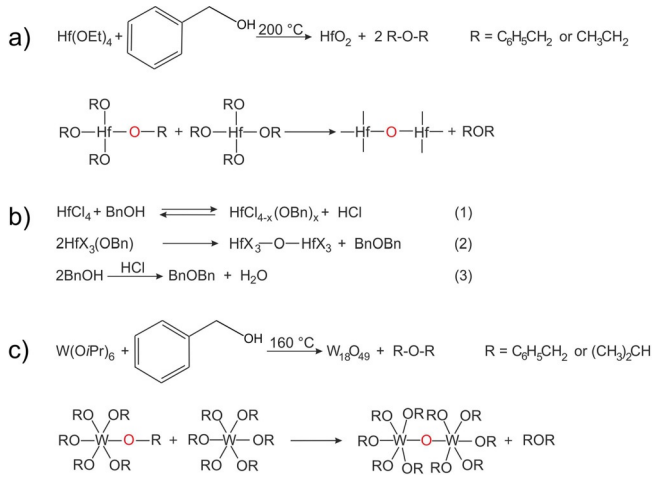

Scheme 5. a) Formation of HfO_2 nanoparticles from hafnium ethoxide and benzyl alcohol via ether elimination. b) Proposed mechanisms for Hf-*O*-Hf bond formation via ether elimination (ligands not participating in the reaction are represented by X, BnOH = benzyl alcohol). c) Formation of tungsten oxide nanostructures from tungsten isopropoxide and benzyl alcohol via ether elimination.

A two-step mechanism was proposed based on the NMR analysis of the final reaction mixture, which showed the presence of organic ethers. In a first step, the addition of hafnium(IV) ethoxide to benzyl alcohol resulted in a partial exchange of the ethoxide ligand against benzyl alcohol. In the next step, Hf-*O*-Hf bonds were formed via condensation of the alkoxides under elimination of organic ethers, mainly dibenzyl ether.

Driessche and co-workers proposed a similar dibenzyl ether elimination mechanism for the microwave assisted synthesis of cubic ZrO_2 nanocrystals from $Zr(OiPr)_4$ and benzyl alcohol, based on GC-MS analysis.[117] Ether elimination remained the main reaction pathway even if the synthesis was performed in a 1.5 L batch reactor.[158] Zimmermann and Garnweitner studied the formation of anatase nanoparticles by the reaction of titanium(IV) isopropoxide in benzyl alcohol following an ether elimination pathway. Besides the ether elimination byproducts spontaneous water release due to catalytic condensation of benzyl alcohol to dibenzyl ether at the Ti center led to an increase of pressure in the reaction system causing instant nucleation and fast growth of the crystalline anatase nanoparticles.[159] According to ^1H NMR data, an analogous ether elimination reaction was also found for the formation of anatase TiO_2 nanoparticles prepared from the reaction of titanium isopropoxide with benzyl alcohol on the surface of carbon nanomaterials using microwave heating.[160] The solvothermal reaction between titanium(IV) *tert*-butoxide and benzyl alcohol led to the elimination of di-*tert*-butyl ether and benzyl ether.[157]

An interesting observation was made during the synthesis of tungsten oxide nanowires from tungsten isopropoxide in benzyl alcohol. While the first step followed the common ether elimination mechanism (Scheme 5c), in a next step the formed tungsten oxide nanowires catalyzed the polymerization of benzyl alcohol into polyphenylene methylene (Figure 5a)

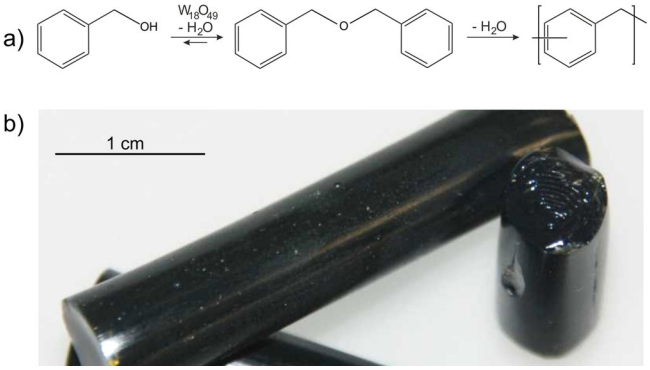

Figure 5. a) Tungsten oxide catalyzed formation of polyphenylene methylene from benzyl alcohol and dibenzyl ether. b) Photograph of a tungsten oxide nanowire-poly(phenylene methylene) monolith.

under their incorporation into the polymer, forming an inorganic-organic hybrid monolith (Figure 5b).[47] A similar polymerization reaction was also observed in the WCl_6–benzyl alcohol[161–162] and in the $FeCl_3$–benzyl alcohol system.[144] Interestingly, it was found that the resulting polymer polyphenylene methylene exhibits pronounced blue fluorescence in spite of the fact that the methylene group prevents full conjugation.[163] The explanation for this effect lies in the overlap of *p*-orbitals across repeat units, in the so-called homoconjugation.[163]

Ether elimination reactions were also observed starting from metal chlorides as precursors and benzyl alcohol via in situ formation of the metal alkoxide species (Scheme 2a). De Roo et al. investigated the reaction mechanism between $HfCl_4$ and benzyl alcohol in both the autoclave and in the microwave reactor using GC-MS and NMR analyses.[164] The proposed formation mechanism involved a two-step process (Scheme 5b). In the first step, a ligand exchange took place, where the chloride was partly replaced by benzyl alcoholate (Scheme 5b, (1)). In the second step, the oxygen was transferred to the metal center via elimination of dibenzyl ether (Scheme 5b, (2)). The HCl produced during the ligand exchange reaction (1) acted as

a catalyst for the condensation of benzyl alcohol into dibenzyl ether and H_2O (Scheme 5b, (3), and also Scheme 4 (6)), which explained the formation of dibenzyl ether in extensive stoichiometric excess. It is interesting to note that the microwave-assisted synthesis produced smaller and monodisperse HfO_2 nanoparticles in shorter reaction times compared to the autoclave synthesis, while the basic reaction mechanism remained the same. A similar dibenzyl ether elimination mechanism was proposed for the synthesis of monoclinic ZrO_2 nanocrystals from $ZrCl_4$ in benzyl alcohol.[117] Change of the precursor from $ZrCl_4$ to $Zr(OiPr)_4$ altered the crystal phase from monoclinic to cubic zirconia. Based on the GC-MS analysis, the authors found that the change in crystal structure originated from a different reaction mechanism induced by the release of HCl during synthesis.[117] Wang et al. reported the synthesis of single crystalline $TiOF_2$ nanocubes with a mesoporous structure using benzyl alcohol as solvent. During the reaction, alcoholysis of TiF_4 resulted in the formation of $(RO)_xTiF_{4-x}$ and HF. The release of HF as a strong acid during the reaction catalyzed the condensation between two benzyl alcohols to benzyl ether and H_2O. The growing concentration of H_2O with the reaction time resulted in the hydrolysis of $(RO)_xTiF_{4-x}$ and formation of $TiOF_2$ nanocrystals, which finally transformed into anatase TiO_2.[138]

4.2.2 C–C bond formation

Under alkaline reaction conditions or in the presence of Lewis acidic species, the reaction between metal alkoxides and alcohols undergoes a Guerbet-type C–C coupling rather than an ether elimination. Such a C–C bond formation was observed between benzyl alcohol and the isopropoxy ligand during the synthesis of $BaTiO_3$ (Scheme 6a) and $SrTiO_3$ nanoparticles from the reaction between the respective alkaline earth metals, $Ti(OiPr)_4$ and benzyl alcohol.[57] Benzyl alcoholate, which is produced from the reaction between metallic barium and benzyl alcohol (Scheme 6b), plays the role of the base during the reaction (Scheme 6c). The deprotonation of the β-carbon of the isopropoxy ligand by benzyl alcoholate changes the reaction path towards C–C bond formation. The nucleophilic attack of a β-carbon atom (carbanion) of the isopropoxide onto the benzyl group, which is activated by an interaction of the OH group of the alcohol with titanium, leads to the formation of a titanium complex with a coordinated 4-phenyl-2-butoxide and an OH group. The Ti-OH group promotes further condensation under release of the alcohol and formation of metal-oxygen-metal bridges. Although not much information about the crystallization pathway of $BaTiO_3$ is known, it is clear that such a molecular scheme is greatly simplified and that it does not consider the interaction between the Ti and Ba species.

Ten Elshof et al. studied the formation mechanism of $BaTiO_3$ nanoparticles in benzyl alcohol in more details, however using barium hydroxide octahydrate as barium source, which renders the process hydrolytic.[165] Nevertheless, they made some observations that might be interesting for nonhydrolytic processes, too. When reacting $Ti(OiPr)_4$ with benzyl alcohol they found that at room temperature three and at elevated temperature all four isopropoxide ligands were replaced by benzyl alcohol.

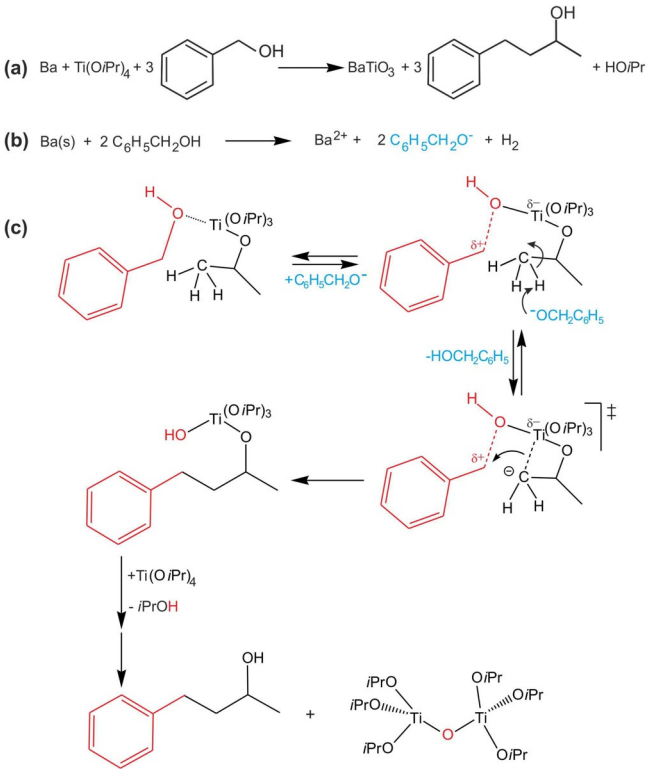

Scheme 6. Proposed reaction mechanism for the formation of $BaTiO_3$ nanoparticles in the reaction system Ba-$Ti(OiPr)_4$-benzyl alcohol: (a) Overall reaction equation, (b) reaction of metallic barium with benzyl alcohol, and (c) formation of a Ti-*O*-Ti bridge and 4-phenyl-2-butanol via C–C bond formation between benzyl alcohol and isopropoxy ligand. Scheme (c) reproduced from ref. [1].

This is an important observation, because the benzyl alcoholate complex has a different reactivity than the initial titanium isopropoxide. Furthermore, the authors indeed found a strong interaction between the titanium alkoxide and the barium salt, and the third result was that all $BaTiO_3$ nanoparticles, even under different reaction conditions, had approximately the same crystal size of about 7–9 nm. This effect was explained by the highly growth limiting effect of benzyl alcohol, which acted as a capping layer. The reason was the packing density of benzyl alcohol molecules on the surface of the nanoparticles, which depended on the curvature and thus on the size. The packing density of benzyl alcohol was proposed to be lower on small crystals, promoting further growth, while at a crystal size of 7–9 nm the packing density was so high that growth by monomer attachment was heavily restricted.[165]

In comparison to most of the metal oxide nanoparticles produced by the benzyl alcohol route, the rare earth oxides behave somewhat peculiar. Instead of forming discrete inorganic nanoparticles, they grow into highly ordered lamellar organic-inorganic nanohybrids with organic species intercalated in between the crystalline metal oxide layers.[48] The source of the organic component can be twofold: Either it is already present in the initial reaction solution or it is formed in situ during the reaction course. In either case, the organic species through its coordination properties strongly influences the

growth behavior of the inorganic phase, favoring anisotropic crystal morphologies.

The synthesis of yttria nanohybrids is one of those examples, where the organic component was formed in situ.[46] The reaction between $Y(OiPr)_3$ and benzyl alcohol followed a C–C coupling mechanism driven by the Lewis acidity of the yttrium ion.[46] NMR analysis revealed the presence of 4-phenyl-2-butanol, indicating a similar mechanism like for $BaTiO_3$. However, in the case of yttria, the deprotonation of the isopropoxy ligand could not be due to the alkaline conditions. Instead, the high Lewis acidity of the yttrium ions enhanced the attraction of electrons, favoring deprotonation of the $-CH_3$ group of the isopropoxy ligand. The carbanion, stabilized by an agostic bond to the yttrium center, then reacted with the benzyl fragment through the formation of 4-phenyl-2-butoxide and a metal-bound hydroxyl group. Further condensation led to Y-*O*-Y bond formation under the release of 4-phenyl-2-butanol. In addition to the C–C coupling reaction, the authors also observed two hydride-transfer reactions, which had a tremendous effect on the structure. Catalyzed by yttria, benzyl alcohol was transformed into benzoic acid and toluene. The benzoate molecules coordinated to the yttrium oxide surface, blocking further attachment of monomers, and this geometrical restriction of the crystal growth finally resulted in the formation of a lamellar organic-inorganic nanohybrid.[46]

4.3 Reactions between metal alkoxides and amines

Benzyl alcohol is an extremely versatile oxygen source for the formation of metal oxide nanoparticles. Similarly, benzyl mercaptan and other mercaptans have successfully been used as sulfur donor for the synthesis of various metal sulfides.[40,166] Accordingly, one could assume that benzylamine might be able to act as nitrogen donor for the formation of metal nitrides. Unfortunately, most of the reactions in benzylamine still result in metal oxide nanoparticles[167] with the only exception being copper nitride.[42]

The reaction between titanium isopropoxide and benzylamine gave access to anatase nanoplatelets, stacked together in a lamellar fashion with a small organic layer in between.[168] Based on GC-MS analyses the condensation between two benzyl amine molecules represented the main reaction during solvothermal processing and led to the formation of dibenzylamine and ammonia. However, the ammonia obviously failed to induce bridging between the metal centers, and thus the thermodynamically more stable oxide formed rather than the nitride. As oxygen source for Ti-*O*-Ti bond formation, elimination of propene from the isopropoxy ligand was proposed, producing a Ti-OH species, which then can undergo further condensation.[168]

In contrast to titanium isopropoxide, the reaction between the copper alkoxide $Cu(OCH_3)_2$ and benzylamine indeed led to the formation of copper nitride rather than copper oxide.[42] GC-MS data indicated that initially a benzylamine molecule reacted with two $Cu(OCH_3)_2$ to yield methanol, $CuOCH_3$ and benzenemethanimine (Scheme 7, Equation (1)). The high Lewis basicity of benzylamine effectively solvated the Cu^{II} ions and the high oxidation efficiency of Cu^{II} ions was responsible for oxidation of benzylamine to benzenemethanimine. The benzenemethanimine reacted further with benzylamine to form *N*-benzylidenebenzylamine and ammonia (Scheme 7, Equation (2)), and the ammonia together with $CuOCH_3$ immediately transformed into Cu_3N and methanol (Scheme 7, Equation (4)). The strong basicity of the methoxide ions is the driving force for the nitridation reaction. The oxidation of benzenemethanimine to benzonitrile by $Cu(OCH_3)_2$ led to the formation of trace amounts of benzonitrile and again $CuOCH_3$ (Scheme 7, Equation (3)).

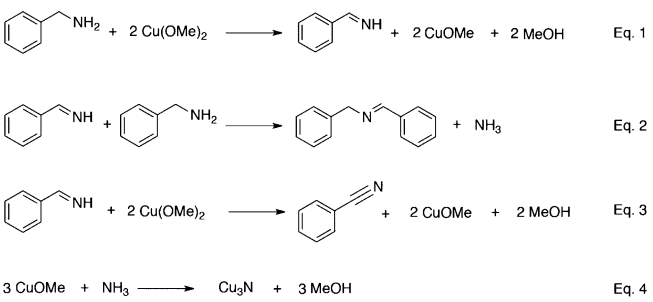

Scheme 7. Proposed reaction mechanism for the main processes involved in the formation of Cu_3N nanoparticles ($Me = CH_3$). Reprinted with permission from ref. [42]. Copyright (2015) American Chemical Society.

4.4 Reaction between metal acetylacetonates and alcohols

Metal acetylacetonates are viable alternatives to metal halide or alkoxide precursors due to their stability and better availability. The solvothermal reaction between metal acetylacetonates and benzyl alcohol allows the preparation of nanocrystalline Fe_3O_4,[169] ZnO,[170] as well as metallic copper nanoparticles.[77] In comparison to $BaTiO_3$ and yttria, the organic byproduct is not 4-phenyl-2-butanol, but 4-phenyl-2-butanone. The detailed mechanism has already been reported.[1] The presence of 4-phenyl-3-buten-2-one in the final reaction solution as an oxidation product of 4-phenyl-2-butanone indicated that 4-phenyl-2-butanone was able to partly reduce Fe^{III} to Fe^{II}, which was required for the formation of Fe_3O_4. In this context it is interesting to refer to a study of Fontanesi et al., who rationalized this mechanism from a theoretical point of view by Density Functional Theory.[171]

Cleavage of the acetylacetonate ligand also occurred in the case of ZnO nanoparticle formation. The reaction between zinc acetylacetonate hydrate and various alcohols including 1,4-butanediol,[172] 1-butanol, isobutanol,[173] and benzyl alcohol[170] was found to proceed through the formation of a zinc enolate complex as an intermediate during alcoholysis of acetylacetonate. Orel and co-workers reported the synthesis and the underlying reaction mechanism of ZnO nanoparticle formation upon refluxing an oversaturated solution of zinc acetylacetonate hydrate in 1-butanol and isobutanol.[173] The authors proposed a mechanism for Zn-*O*-Zn bond formation based on ^1H and ^{13}C NMR analysis of the final reaction solution after precipitation of the ZnO (Scheme 8a). The alcohol molecule nucleophilically attacked the electron deficient carbonyl carbon of the acetylacetonate ligand (1), which was activated by the

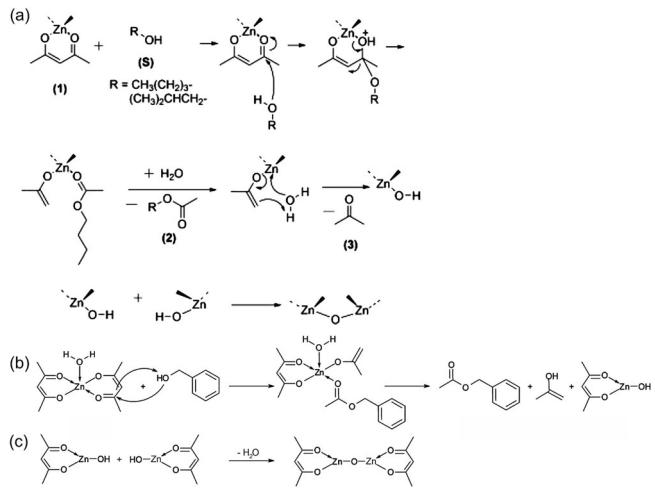

Scheme 8. Proposed mechanism of Zn-*O*-Zn bond formation from zinc acetylacetonate hydrate and (a) 1-butanol or isobutanol and (b–c) benzyl alcohol. Scheme (a) reproduced from ref. [173] with permission of Elsevier. Scheme (b) and (c) reproduced from ref. [34].

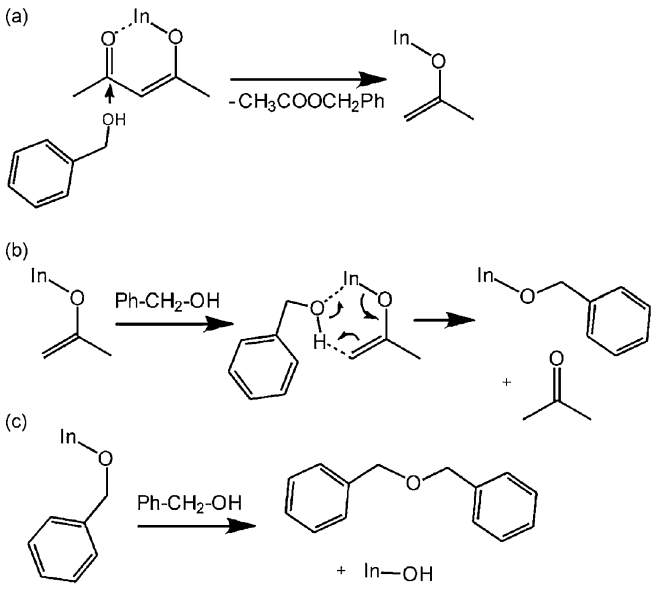

Scheme 9. Main reaction pathway for the formation of the hydroxy species upon reaction of $In(acac)_3$ with benzyl alcohol. Scheme reproduced from ref. [175].

electropositive zinc precursor center. The cleavage of the C–C bond led to butyl acetate and isobutyl acetate (2), respectively, and an enolate ligand. The next step proceeded via the nucleophilic attack of the water molecule, present in the hydrated precursor, on the zinc center. The proton transfer from the water molecule to the enolate ligand resulted in the elimination of acetone (3) and formation of Zn-OH species, which finally underwent condensation to Zn–*O*–Zn. Ludi et al. proposed a similar mechanism for the formation of fan- and bouquet-like ZnO nanostructures from zinc acetylacetonate hydrate in benzyl alcohol based on the GC-MS analysis of the reaction solution (Scheme 8 b, c).[170] Damm et al. proposed an analogues C–C cleavage mechanism with the elimination of acetone and ester for the formation of Al-doped ZnO nanoparticles by the thermal decomposition of the metal acetylacetonates with 1,2-hexadecanediol. In addition to acetone, thermal decomposition products of ester such as acetic acid, a mixture of alkanes and alkenes, carbon dioxide and water were detected using headspace GC analysis during the synthesis of ZnO:Al nanoparticles.[174]

Zhang et al. developed a nonaqueous route for the synthesis of phase-pure transition metal niobates ($InNbO_4$, $MnNb_2O_6$, and $YNbO_4$) based on the solvothermal reaction of niobium chloride and the corresponding transition metal acetylacetonates in benzyl alcohol.[175] The chemical mechanisms responsible for the oxygen supply were based on three almost simultaneously occurring processes as shown in Scheme 9: a) A metal promoted alcoholysis of the acetylacetonate ligand leading to the formation of an enolate and benzyl acetate, b) release of acetone through the coordination of benzyl alcohol to the metal center, and c) benzyl ether elimination catalyzed by the niobium center. The ether elimination occurred only in the presence of $NbCl_5$, which was hydrolyzed by the formed water.

Tyagi and co-workers achieved the synthesis of 4–8 nm SnO_2 nanocrystals via reaction between $Sn(acac)_2Cl_2$ and benzyl alcohol at 200 °C.[176] Based on NMR and GC-MS analyses, the proposed mechanism involved ether elimination as main pathway accompanied by alcoholysis of acetylacetonate ligand bound to the metal center. Initially, partial exchange of the chloride ligands at the precursor by benzyl alcohol resulted in the formation of tin alkoxides and HCl (cf. Scheme 2 a). The condensation between two tin alkoxides led to Sn-*O*-Sn bonds with elimination of dibenzyl ether (cf. Scheme 3 c). The HCl formed during the exchange reaction catalyzed the alcoholysis of the acetylacetonate ligand by benzyl alcohol to form benzyl acetate and acetone.

Staniuk et al. studied the reaction between Cu(II) acetylacetonate and benzyl alcohol for the synthesis of copper nanoparticles.[77] In situ FTIR, UV/Vis and in situ XAS studies indicated that the nucleation of Cu_2O co-occurred with the formation of benzyl acetate through the reaction of acetylacetonate with benzyl alcohol and formation of benzaldehyde through the oxidation of benzyl alcohol with concurrent reduction of Cu^{2+} to Cu^{+}. The Cu_2O nanoparticles transformed by solid-state reduction to metallic copper, which was accompanied by oxidation of benzyl alcohol to benzaldehyde.

4.5 Reaction between metal acetylacetonates and amines

The reaction between metal acetylacetonates and amines provides an effective pathway for the synthesis of various metal oxide nanoparticles.[167,177–181] The solvothermal reaction between metal acetylacetonates and benzylamine, for example, offers a general nonaqueous pathway for the synthesis of metal oxide nanoparticle including iron, indium, gallium and zinc oxide.[167] By analyzing the reaction byproducts using GC-MS, the authors proposed a chemical formation mechanism involving nucleophilic attack of benzylamine on one of the carbonyl groups of the acetylacetonate, leading to the cleavage of the C–C bond and formation of *N*-benzyl acetamide and an

enolate ligand coordinated to the metal center. In this case, the enolate ligand functioned as an electrophile, which is in contrast to the reaction of iron(III) acetylactonate with benzyl alcohol, where the enolate ligand acted as the nucleophile. A nucleophilic attack of benzylamine on the electrophilic carbon of the enolate led to the formation of an imine and Fe–OH, which further condensed to form Fe-*O*-Fe bonds and finally to the crystalline network of the oxidic nanoparticles. A more detailed discussion and a reaction Scheme of this reaction mechanism can be found somewhere else.[1,34,167]

Recently, Karmaoui et al. proposed a very similar reaction mechanism for the synthesis of In_2O_3 nanoparticles using indium(III) acetylacetonate and *n-butyl*amine under solvothermal conditions.[178] The mechanism proceeded analogously through the formation of an indium enolate and *N*-butylacetamide. In the next step, the indium enolate ligand underwent nucleophilic attack from another amine, resulting in In-OH and *N*-butylpropan-2-imine. Finally, the nucleophilic attack of the hydroxyl group of In-OH onto the indium site in indium acetylacetonate led to the formation of In-*O*-In bonds under elimination of acetylacetone, which condensed with another amine to produce 4-(butylamino)pent-3-en-2-one.

4.6 Ester and amide eliminations

Ester elimination reactions (cf. Scheme 3 b), where an ester is produced as an organic byproduct during the formation of metal oxides, are frequently used for the synthesis of metal oxide nanocrystals. Different combinations of precursors and solvents lead to the elimination of an ester with the formation of M-*O*-M bonds, including the reaction between metal alkoxides and metal carboxylates,[182,183] metal alkoxides and carboxylic acids,[184] metal alkoxides and organic acid anhydrides,[185] and metal acetates and alcohols.[186] In some reactions, however, the ester elimination is a result of the reaction between a solvent mixture of alcohol and carboxylic acid (which has, by the way, a long history,[187] but is still nowadays used[188]), leading to the in situ formation of water that reacts with metal alkoxides or metal halides, producing metal oxide nanoparticles. In these cases, although the formation of the metal oxide is expected to be based mainly on hydrolytic processes, nonhydrolytic pathways cannot be excluded.[187,189,190]

The nonhydrolytic reaction between metal alkoxides and metal carboxylates, leading to the formation of metal oxo bridges with concurrent elimination of an organic ester (cf. Scheme 3 b) was reported for the preparation of several metal oxo clusters[182,189] as well as metal oxides.[183,191] Analogously, amide elimination was observed by reacting metal acetates with metal amides. Mathur and co-workers used an acetamide elimination reaction between silicon acetate, $Si(OAc)_4$, and titanium (IV) dimethylamide or diethylamide, $Ti(NR_2)_4$ (R = Me, Et), for the synthesis of titanosilicate xerogels.[192] They compared the xerogels prepared by acetamide elimination reactions with the xerogels prepared by ester elimination from $Si(OAc)_4$ and titanium(IV) isopropoxide and found a significantly higher content of the Si-*O*-Ti bonds in xerogels obtained through amide eliminations. This effect was due to the suppression of the ligand exchange and homocondensation reaction at silicon and at titanium in the acetamide elimination route.

The reaction of metal alkoxides with carboxylic acids offers another route for the synthesis of metal oxides through ester elimination reactions (Scheme 10).[193–195] However, this route is not strictly nonhydrolytic, because the reaction of alcohols (produced by ligand exchange of alkoxy by carboxylate groups (Equation (1))) with carboxylic acids can lead to in situ generation of water (Equation (3)).

$$M(OR)_x + R'COOH \longrightarrow M(OR)_{x-1}(OCOR') + ROH \quad \text{Eq. 1}$$

$$M(OR)_{x-1}(OCOR') + ROH \longrightarrow M(OR)_{x-1}(OH) + R'COOR \quad \text{Eq. 2}$$

$$R'COOH + ROH \longrightarrow R'COOR + H_2O \quad \text{Eq. 3}$$

Scheme 10. Overview of the reactions occurring between metal alkoxides and acids: Ligand exchange reactions between alkoxides and carboxylic acids (Equation (1)), esterification of the coordinated acid (Equation (2)), and water formation upon esterification of the free acid (Equation (3)).

The reaction between alkoxy silanes and acetic acid leads to the formation of silica esters (CH_3COOSi-) via the exchange reaction of the acetic acid with the alkoxy group, and the reaction between this silica ester and ethanol yields Si-OH groups and ethylacetate $CH_3COOC_2H_5$.[196,197] The esterification reactions between titanium alkoxides and carboxylic acids allows the synthesis of titanium oxo-isopropoxo clusters[198] as well as titania nanoparticles or nanorods.[184,193,199–202] Long chain carboxylic acids like oleic acid not only act as reactant for esterification, but also as capping and structure directing agent.[193,200] Esterification reactions were also applied for atomic layer deposition (ALD) of titania from titanium isopropoxide and acetic acid.[203] In situ FTIR and ex situ X-ray photoelectron spectroscopy investigations confirmed the formation of surface acetate species via ligand exchange of the alkoxy group by carboxylates (with the elimination of the corresponding alcohol) during the acetic acid pulse, followed by the elimination of ester, and formation of Ti-*O*-Ti bonds during the titanium isopropoxide pulse. This reaction pathway agreed with the mechanism already suggested by Pinna and co-workers before.[204]

The reaction of metal alkoxides with organic acid anhydrides offers another completely nonhydrolytic route to metal oxide nanoparticles. The reaction pathway involves the in situ generation of carboxylates with the elimination of an ester, which can then undergo condensation reaction with an alkoxy group (cf. Scheme 3 b) to form M-*O*-M bonds.

Pande and Mehrotra found that the reaction between titanium isopropoxide and acetic anhydride yielded Ti-*O*-Ti bonds with the elimination of isopropylacetate.[185] This nonhydrolytic anhydride route has later been used for the synthesis of silica[205] and titania.[206,207]

In addition to metal alkoxides and metal carboxylates, and metal alkoxides and acids/acid anhydrides, the reaction of metal carboxylates and alcohols represents the third possibility to synthesize metal oxide nanoparticles by ester elimination.[208] Metal carboxylates are readily available precursors and

easier to handle than the moisture sensitive, and often also very expensive metal alkoxides.

The esterification of the zinc carboxylates, in particular zinc acetate, with alcohols has been widely studied for the synthesis of ZnO as well as doped ZnO nanoparticles with different morphologies, high doping levels and with a broad range of properties.[209–214] Bilecka et al. presented a detailed study of kinetic and thermodynamic aspects involved in the microwave-assisted synthesis of ZnO nanoparticles from zinc acetate and benzyl alcohol.[186] An ester elimination pathway was proposed for the formation of ZnO after GC-MS analysis of the reaction solution (Scheme 11). The formation of benzylacetate and Zn-

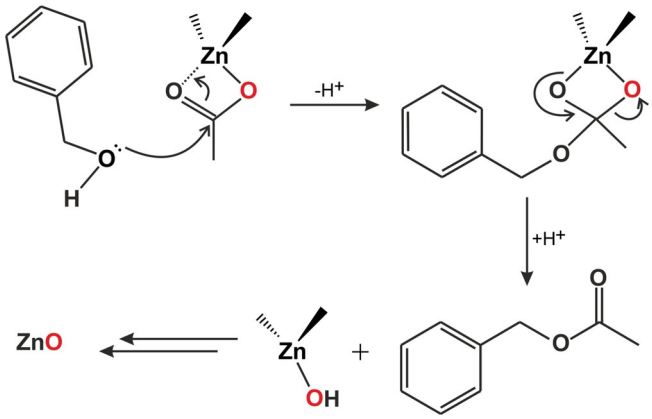

Scheme 11. Reaction of zinc acetate with benzyl alcohol under elimination of benzyl acetate and formation of Zn-OH, which further reacts to ZnO. Adapted with permission from ref. [186]. Copyright (2009) American Chemical Society.

OH was found to be the key step, as the nucleation of the ZnO clusters only occurred, when the Zn-OH concentration reached supersaturation. The growth of the ZnO nanoparticles followed the Lifshitz–Slyozov–Wagner model for coarsening, pointing to a diffusion-limited process.

Hutchison and co-workers developed an esterification pathway for the synthesis of monodispersed In_2O_3, indium tin oxide (ITO), γ-Fe_2O_3, Mn_3O_4, CoO, and ZnO nanocrystals using the corresponding metal acetates as precursors, oleyl alcohol as a solvent and oleic acid as a ligand and shape control reagent.[215] Gaspera et al. reported the ester elimination reaction for the synthesis of ZnO nanocrystals doped with Al, Ga or In by using zinc stearate, the corresponding metal acetylacetonate as precursor for the dopant, oleic acid and 1-dodecanol as ligand and activating agent, respectively.[210] The ligation of the oleic acid at the nanocrystal surface helped to define the crystal shapes[215] and rendered the as-synthesized nanocrystals dispersible in organic solvents.[210]

Analogous to ester elimination is the amide elimination, involving aminolysis of metal carboxylates.[216] Amines (benzylamine or long chain primary amines) act as reactants and capping agents for the shape controlled synthesis of metal oxide nanostructures.[217–219] The synthesis of facet controlled ZnO nanocrystals was achieved through the reaction of zinc acetate and benzylamine.[220] After coordination of benzylamine to Zn^{2+}, forming a Zn(acetate)$_2$-benzylamine complex, aminolysis between benzylamine and the acetate group occurred to form zinc hydroxide and *N*-benzylacetamide. Finally, zinc hydroxide was transformed into ZnO through dehydration.

In this section we discussed ester and amide elimination from metal alkoxides and metal carboxylates. However, also metal acetylacetonates are able to undergo ester and amide elimination, as discussed in Section 4.4 and 4.5, however, in these cases involving C–C bond cleavage of the acetylacetonate ligands. Furthermore, ester and especially amide elimination might play an important role in reaction mixtures containing long-chain carboxylates and amines as stabilizing surfactants. In such cases, it is often forgotten that surfactants can react with each other, heavily influencing the chemical environment and thus nanoparticle formation.

4.7 Reactions of different precursors with ketones and aldehydes

In addition to alcohols and amines, carbonyl compounds such as ketones or aldehydes are also suitable solvents for the non-aqueous synthesis of metal oxide nanoparticles.[81,179,221] Different precursors (usually metal alkoxides) react with ketones and aldehydes via an aldol condensation mechanism, catalyzed either by the Lewis acid or the basic character of the precursor, supplying oxygen to the growing metal oxide clusters or nanoparticles under formation of α,β-unsaturated carbonyl compounds (Scheme 1 c).

Sanchez and co-workers synthesized titanium-oxo clusters through the reaction of Ti(O*i*Pr)$_4$ with ketones such as acetone, acetylacetone and diacetone alcohol at room temperature.[222] They proposed a reaction pathway as shown in Scheme 12 based on NMR analysis of the organic condensation products detected in the acetone system. In a first step, due to the Lewis acid properties of titanium isopropoxide, a Lewis adduct was formed between the carbonyl group of acetone and a titanium center (1). This adduct upon deprotonation led to a titanium-enolate complex (a) with concurrent formation of isopropanol. In a next step, the enolate ligand nucleophilically attacked another acetone species (2), forming a titanium diacetone alcoholate (b), which can either lead to hydroxylation of the titanium center and formation of mesityl oxide (3′), or undergo further condensation reaction with a third acetone molecule (3). In the latter process, the complex b′ is transformed into the tridentate ligand c′.

Goel et al. proposed an analogous mechanism for the reaction between Zn[OC(CH$_2$CH$_3$)$_3$]$_2$ and acetone at room temperature. However, in this case the aldol condensation reaction was catalyzed by the basic nature of the Zn-containing precursor. The reaction proceeded through the deprotonation of acetone, leading to a zinc enolate complex. In a next step, the enolate ligand nucleophilically attacked another acetone species via aldol condensation, ultimately liberating Zn-OH and mesityl oxide as condensation product.[223] Garnweitner et al. reported the synthesis of crystalline anatase nanoparticles via the solvothermal reaction between Ti(O*i*Pr)$_4$ and simple ketones and aldehydes. For the reaction of Ti(O*i*Pr)$_4$ with acetone at 130 °C,

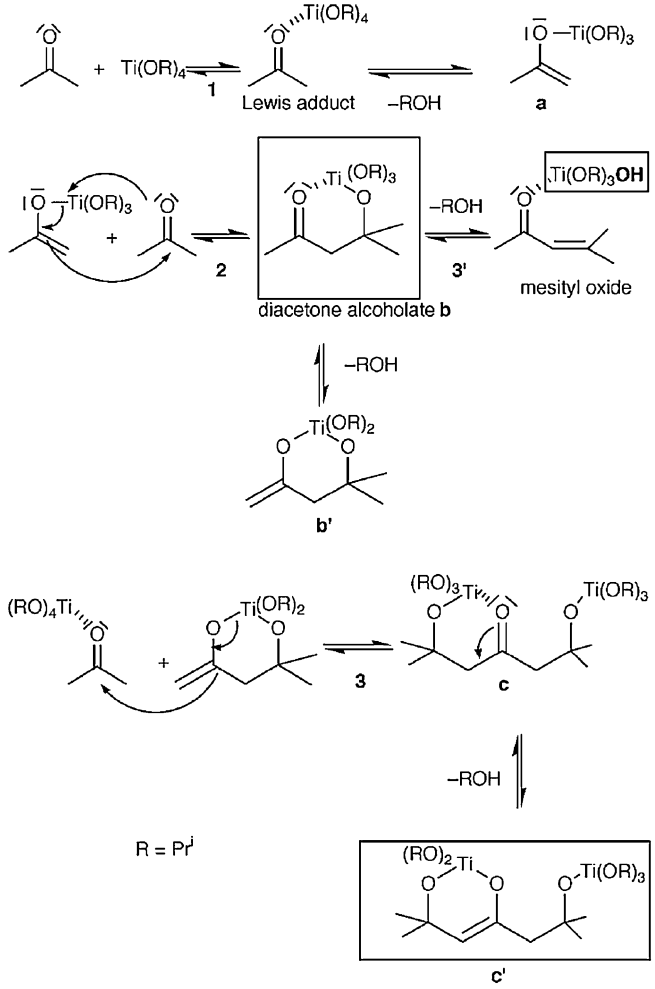

Scheme 12. Proposed mechanism for the aldol condensation reactions between $Ti(OiPr)_4$ and acetone leading to titanium-oxo clusters. Reproduced from ref. [222] with permission from the Centre National de la Recherche Scientifique (CNRS) and The Royal Society of Chemistry.

the authors found that in addition to isopropyl alcohol and mesityl oxide, higher condensation products of acetone such as mesitylene and phorone were also produced during the reaction.[224] Using ^{13}C NMR analysis, Liu et al. identified several aldol condensation products of acetone (mesityl oxide, phorone and mesitylene) in the solution after the solvothermal synthesis of high surface area mesoporous TiO_2 microspheres through the reaction of titanium isopropoxide with acetone at 200 °C.[225]

As a side reaction, especially in the case of higher aliphatic ketones like 2-butanone and 3-pentanone, titanium isopropoxide can undergo a Meerwein–Ponndorf–Verley (MPV) like reaction, where the isopropoxide ligand is oxidized to acetone, whilst the ketone is reduced to an alkoxide group.[224] The mechanism for the oxidation–reduction reaction via hydride transfer is shown in Scheme 13. In the first step, the carbonyl oxygen coordinates to the titanium center (1), followed by the hydride transfer from the α-position of the isopropoxide ligand to the carbonyl group via a six-membered cyclic transition state (2). The reduced ketone binds to the Ti center as an alk-

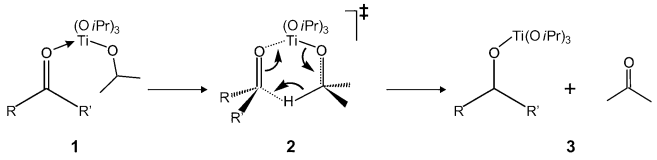

Scheme 13. Side reaction observed during the formation of TiO_2 nanoparticles in higher aliphatic and aromatic ketones, analogous to the Meerwein–Ponndorf–Verley reaction. Scheme reproduced from ref. [226].

oxide and acetone is released (3). This reaction does not contribute to the formation of the metal oxide, however, it is a prerequisite for the synthesis of titania nanoparticles in solvents like benzophenone, which do not possess any α-H atoms necessary for aldol condensation reactions. For example, benzophenone reacted with $Ti(OiPr)_4$ via MPV-like process, producing benzhydrol and acetone. The released acetone condensates with another benzophenone to 4,4-diphenyl-3-buten-2-one, providing the oxygen needed for titania formation.[224]

The MPV-like and aldol condensation reactions were also found during the synthesis of lanthanum hydroxide via the reaction of $La(OiPr)_3$ and $KMnO_4$ with a mixture of benzyl alcohol and 2-butanone.[227] The proposed pathway, based on NMR and gas chromatography analyses, involved a MPV-like reaction between the isopropoxide ligand and 2-butanone, leading to the reduction of 2-butanone to 2-butanol with concurrent oxidation of the isopropoxy ligand to acetone. The metal coordinated enol tautomer of acetone induced the aldol condensation with 2-butanone, leading to the formation of a metal hydroxide species and 4-methyl-3-hexen-2-one. The solvothermal synthesis of amorphous lead zirconate titanate powders via the reaction of lead(II) acetylacetonate with zirconium/titanium isopropoxide in 2-butanone also involved MPV-like oxidation-reduction producing 2-butanol and acetone.[228] The formation of the inorganic network occurred via the aldol condensation reactions of 2-butanone with itself and with acetone, leading to the formation of 5-methyl-4-heptene-3-one and 5-methyl-4-hexene-3-one, respectively. The reaction of a crystalline barium titanium oxo alkoxide with acetone at room temperature allowed the synthesis of $BaTiO_3$ nanoparticles. Also here, the aldol condensation reaction supplied the oxygen for condensing the oxo alkoxide clusters. When the reaction was carried out in cyclohexanone, the MPV-like side reactions took place, in addition to aldol condensation.[229] Niederberger et al. reported the synthesis of $BaTiO_3$ nanoparticles by the solvothermal reaction between metallic barium, dissolved in acetophenone, and titanium isopropoxide.[230,231] The reaction of metallic barium with acetophenone formed barium enolates and hydrogen gas. After the addition of titanium isopropoxide, the enolate coordinated to the titanium center. During solvothermal treatment, the enolate attacked a second acetophenone, similar to an aldol coupling mechanism, leading to the formation of 1,3-diphenyl-2-buten-1-one, isopropanol and a Ti-OH group, which then further condensed to form $BaTiO_3$ nanoparticles. Typically, the acetophenone needs to be degassed before use to avoid formation of $BaCO_3$ as a side product.[231] Wu et al. reported the synthesis of titania nanomaterials from

the reaction of $TiCl_4$ and acetone or other ketones via aldol condensation reactions.[232] Depending on the molar ratio of $TiCl_4$ to acetone, TiO_2 with different phases and morphology were produced. $TiCl_4$ acted as a Lewis acid, catalyzing the aldol condensation reaction of acetone to form diacetone alcohol, which can easily dehydrate to produce mesityl oxide and its isomers. The dehydrated dimers further condensate with the remaining acetone to produce varying amounts of dehydrated trimers, tetramers, etc. The controlled hydrolysis of $TiCl_4$ by the in situ generated water molecules from the dehydration of acetone led to the formation of TiO_2. Kränzlin et al. studied the crystallization mechanism of different polymorphs of titania in the $TiCl_4$-acetone system.[233] However, these results are discussed in more details in Section 5. Li et al. synthesized TiO_2 microspheres via a one-pot template-free solvothermal reaction of tetra-*n*-butyl titanate with acetylacetone.[234] The authors proved the occurrence of aldol condensation and Robinson cyclization reactions by mass spectrometry, ^{13}C-NMR and FTIR studies. The solvothermal reaction of Ni(II) acetylacetonate with 2-butanone also followed the aldol condensation mechanism, giving access to NiO nanoparticles.[235] Using GC-MS and FTIR analysis of the reaction byproducts, the authors confirmed the formation of condensation products of 2-butanone.

Aldehydes such as benzaldehyde can also be used as oxygen source in the nonaqueous synthesis of TiO_2 nanoparticles starting from Ti(O*i*Pr)$_4$.[224] The identified reaction byproducts included benzyl alcohol (a reduction product of benzaldehyde), benzyl benzoate (a disproportionation product of benzaldehyde), 4-phenyl-2-butanone (3), and 4-phenyl-3-buten-2-one (5), as shown in Scheme 14. In a first step, a MPV-like reaction of benzaldehyde with Ti(O*i*Pr)$_4$ led to acetone and benzyl alcohol (1). Next, in pathway 1, benzyl alcohol reacted with another isopropoxy ligand via the C–C coupling reaction. The resulting 4-phenyl-2-butanol (2) was readily oxidized to 4-phenyl-2-butanone (3). In pathway 2, the aldol condensation between acetone and benzaldehyde led to the formation of 4-phenyl-3-buten-2-one (5). For aromatic aldehydes, pathway 1 is favored, as the intermediate carbocation is stabilized, whereas for aliphatic aldehydes, aldol condensation reactions in pathway 2 are more probable for TiO_2 formation.

5. Crystallization Mechanisms

Crystallization is a key phenomenon on the way from molecular precursors to the final solid crystalline materials. It defines the size, the shape and the crystal structure of the nanoparticles. The basic process of crystallization falls into two types, classical and nonclassical crystallization, depending on whether an atom/ion-mediated growth or a particle-mediated growth mechanism takes place.[27] In the classical crystallization model, primary building blocks like atoms, ions or molecules nucleate into clusters, which may grow or disintegrate again, depending on the counter play of surface and crystal lattice energies. In nonclassical crystallization, the building units are particles or clusters, which aggregate with each other via oriented attachment and mesocrystal formation.[25,27,236] Oriented attachment describes the spontaneous self-organization of particles in such a way that they share a common crystallographic orientation, followed by fusion of these particles at a planar interface. Mesocrystals are defined as colloidal crystals composed of individual, stabilized, and crystallographically aligned nanocrystals, leading to scattering properties similar to a single crystal.[27] In some cases, mesocrystals are difficult to discriminate from classically grown single crystals, especially when the nanoscale building blocks are perfectly oriented and partially fused. Nevertheless, in comparison to structures formed by oriented attachment, the nanoscale building blocks in mesocrystals remain stabilized, typically by an organic coating, and do not fully fuse together. For an extensive overview of non-classical crystallization mechanisms, we refer the reader to some excellent recent reviews[25,27,28,236–240] and to a textbook.[241] It seems that particle-based crystallization pathways play a particularly

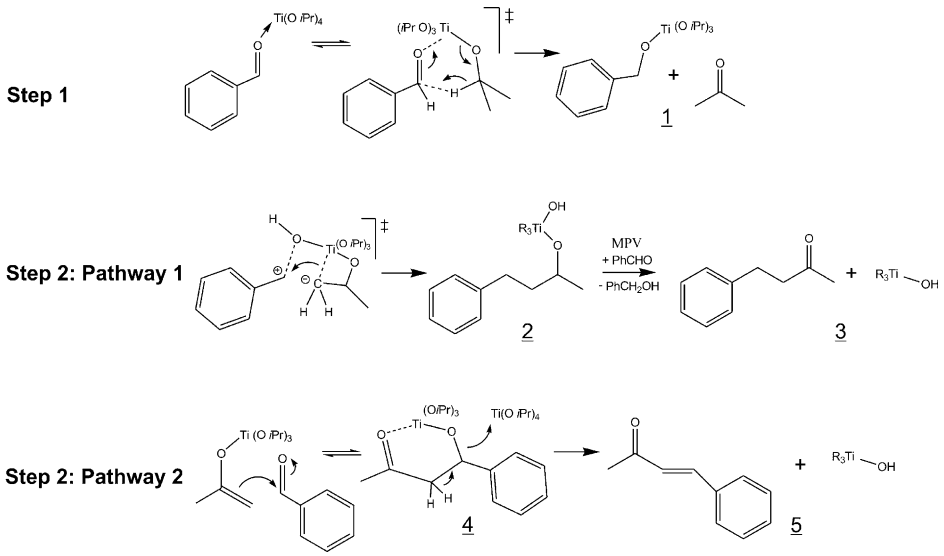

Scheme 14. Proposed reaction pathways leading to the formation of TiO_2 nanoparticles in benzaldehyde. Scheme adapted from ref. [224] with permission of the Royal Society of Chemistry.

important role in nonaqueous environment. As a matter of fact, the few studies available in literature point to rather complex crystallization mechanisms, way beyond the classical nucleation and growth model. However, in spite of the complicated growth modes, the morphology of the final nanostructures can still be amazingly uniform.

We will start our discussion with a few examples on oriented attachment. While oriented attachment of titania nanoparticles can be used to synthesize mechanically self-supporting networks of macroscopic size, e.g., aerogels,[242,243] Dalmaschio and Leite made the unusual observation that oriented attachment of titania can also be reversible.[244] The solvothermal reaction between titanium(IV) butoxide and oleic acid led to the formation of single crystalline TiO_2 nanorods, consisting of several anatase nanocrystal units with truncated bipyramidal Wulff shape. HRTEM investigations after different reaction times showed that the anatase nanocrystals initially underwent oriented attachment, producing nanorods with surfaces dominated by {101} faces (Figure 6a). With increasing reaction times,

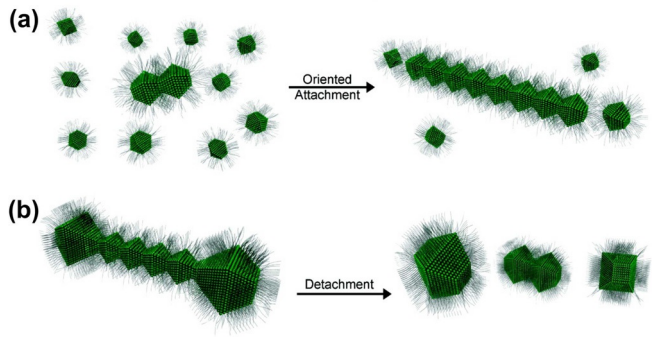

Figure 6. Schematic of (a) the oriented attachment of anatase nanocrystals with tetragonal bipyramidal Wulff shapes into nanorods and (b) nanorod fragmentation by a process similar to Rayleigh instability into well faceted anatase nanoparticles. Reprinted with permission from ref. [244]. Copyright (2012) American Chemical Society.

surface diffusion promoted mass transportation towards the tips of the rods, resulting in dumbbell-like morphologies, which then fragmented by a detachment process into well-faceted nanoparticles (Figure 6b). Also antimony-doped tin oxide (ATO) nanocrystals synthesized by the benzyl alcohol route present an oriented attachment growth mechanism.[245] In that report, the authors showed that the combined use of surface energy ab initio calculations and Wulff construction could be applied to study the oriented attachment configurations. Using $SnCl_4$ and benzyl alcohol for the synthesis of SnO_2, Stroppa et al. observed an unusual anisotropic growth via oriented attachment along the $<110>$ directions, which are equivalent according to the SnO_2 crystallographic structure symmetry.[246]

Oriented attachment can proceed in more than just one direction, leading to 3-dimensional architectures. The solvothermal reaction between tetrabutyl titanate and acetic acid yielded nanoporous anatase TiO_2 mesocrystals with spindle shape.[247] The proposed mesoscale assembly process involved the formation of anatase nanocrystals and their oriented aggregation with incorporation of in situ produced butyl acetate, finally resulting in spindle-shaped anatase mesocrystals. In another study, the solvothermal reaction between $TiCl_4$ and n-octanol resulted in the formation of anatase TiO_2 mesocrystals with a truncated bipyramidal Wulff shape via a kinetically controlled growth mechanism assisted by the oriented attachment process.[248]

As already discussed in the introduction, the study of mechanisms, including chemical reaction and crystallization pathways, makes greatest demands on the analytical probes to be able to provide a full reaction monitoring from the dissolution of the precursor to the final nanoparticles. A particularly illustrative example in this direction was the study of the crystallization mechanism of MoO_2 nanorods by Koziej et al. by reacting MoO_2Cl_2 with a mixture of benzyl alcohol and acetophenone (Figure 7).[81] In situ XAS, XRD, SEM and TEM analyses in-

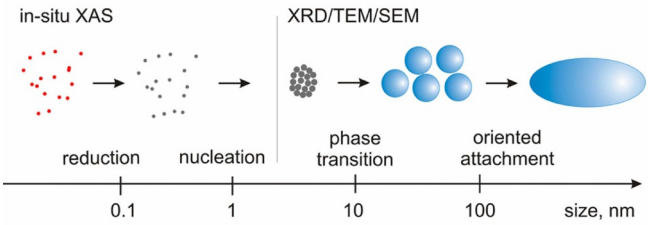

Figure 7. Overview of the formation mechanism of MoO_2 nanorods from MoO_2Cl_2 in a mixture of benzyl alcohol and acetophenone with the corresponding characterization techniques, the size ranges addressed, and the processes involved. Reproduced from ref. [81].

dicated that the crystallization and growth process of MoO_2 nanorods started with the rapid reduction of MoO_2Cl_2 and nucleation of hexagonal MoO_2 nanoparticles of 2 nm in size and with spherical shape. The next two processes occurred simultaneously, namely the aggregation of small nanocrystals into rods via oriented attachment and the transformation from the hexagonal to the monoclinic crystal structure. Time (i.e., size) dependent phase transformations were also observed for indium tin oxide nanoparticles synthesized in benzyl alcohol.[249] The initially formed small nanocrystals, stabilized by an organic matrix, underwent a phase transformation into the bixbyite structure upon crystal growth.

Olliges-Stadler et al. provided an in-depth study on the crystallization processes and morphological aspects of tungstite ($WO_3 \cdot H_2O$) formation through the reaction of tungsten hexachloride with benzyl alcohol.[106] Based on in situ small angle X-ray scattering (SAXS) and time dependent ex situ TEM analysis, the proposed particle-based crystallization process (Figure 8) involved first the crystallization of primary particles (2–8 nm), their assembly into rod-like architectures and the subsequent internal reorganization into crystallographically oriented stacks of platelets. Finally, and rather unexpectedly, the platelet stacks started to fall apart, forming shorter stacks or even individual platelets.

Considering the simplicity of the reaction systems, often composed just of the two compounds precursor and solvent,

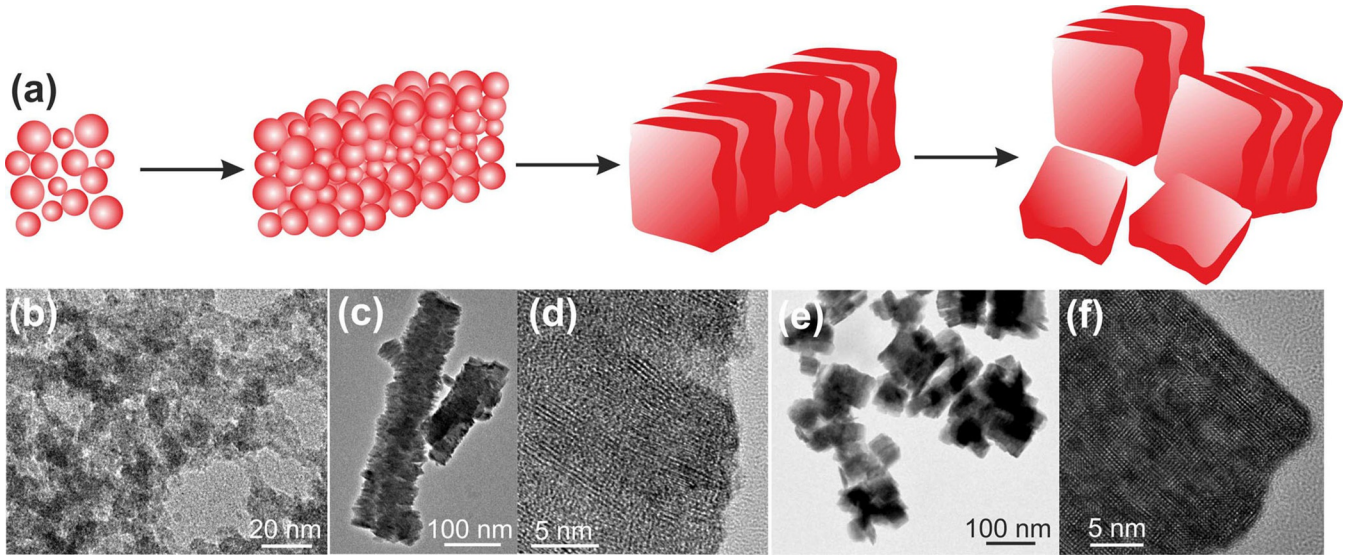

Figure 8. (a) Schematic of the proposed crystallization pathway to tungstite nanoplatelets involving formation of spherical particles, their agglomeration into rod-like structures, internal reorganization into platelets and fragmentation. Time-dependent TEM and HRTEM images (b) after 5 min, (c–d) after 20 min, and (e–f) after 1 h. Reproduced from ref. [34].

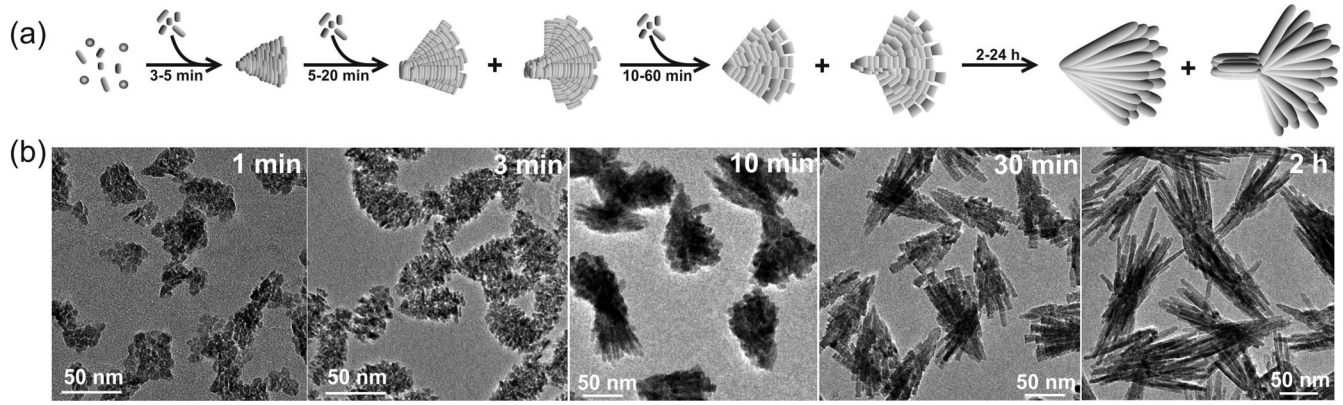

Figure 9. (a) Schematic illustration of the particle morphologies observed after different reaction times during the growth of ZnO nanostructures in benzyl alcohol and (b) corresponding TEM images. Adapted from ref. [170] with permission from the Royal Society of Chemistry.

the chemical as well as the crystallization mechanisms and the final particle morphologies are unexpectedly complex. One example in this category is the formation of fan- and bouquet-like ZnO nanostructures from zinc acetylacetonate hydrate in benzyl alcohol, which followed both a classical and a nonclassical crystallization pathway (Figure 9a).[170] Based on GC-MS analysis, the chemical reaction involved the elimination of benzyl acetate and acetone with the formation of Zn-OH (cf. Scheme 8b). By monitoring the production of benzyl acetate, the authors found that only 0.3% of zinc acetylacetonate hydrate had to react with benzyl alcohol to produce supersaturation in the reaction system and thus to induce nucleation. After one minute of reaction, crystalline ZnO agglomerates were formed (Figure 9b). These agglomerates were transformed into fir tree-like morphologies with a relatively well-defined shape after three minutes of reaction time. Interestingly, most of the nanocrystals within one such structure are crystallographically aligned with respect to each other. After 10 min, and more pronounced after 30 min, the morphology changed again from fir tree-like to angled nanorod bundles, which were connected at one end. The authors proposed that this transition occurred by oriented attachment of newly formed particles along the [0001] direction, thereby establishing nanorod formation by a particle-based mechanism. After 2 h, the ZnO nanostructures reached their final shapes, consisting of well-developed and smooth nanorod bundles. Obviously, the formation mechanism is neither based on the generation of single nanorods and their subsequent assembly, nor on the classical crystal growth mechanism starting from nuclei that grew by ion attachment to the surface. Nevertheless, in spite of a highly concerted mechanism, in which many processes (several nucleation events, oriented attachment, and surface reconstruction) occur parallel in time, it is intriguing to see that the final nanostructures are unexpectedly uniform in size and shape. A review by Ludi et al. provides a comprehensive insight into the nucleation and growth of ZnO nanostructures

in liquid media by classical and nonclassical crystallization pathways.[68] Anatase is able to form rather similar nanorod bundles like ZnO, however, involving a surfactant-assisted sol–gel synthesis and a completely different growth mechanism.[250]

In addition to size and shape, nucleation and growth have also a strong influence on the crystal structure. Accordingly, the study of crystallization mechanisms of metal oxides, which are able to form different polymorphs, is particularly crucial and might help to control the crystal structure during synthesis. One illustrative example in this regard is titania, which crystallizes in different polymorphs depending on the synthesis conditions. If titania is synthesized from $TiCl_4$ and benzyl alcohol, then exclusively anatase nanocrystals formed.[251] In situ powder XRD and SAXS made it possible to probe the kinetics of particle formation, crystallization and aggregation.[252] The data indicated nucleation of crystalline particles with spherical shape and large anisotropic crystal lattice strain, which resulted in anisotropic crystal growth. If the synthesis was performed in acetone rather than in benzyl alcohol, titania precipitated in the anatase and rutile modification. The crystallization was monitored by using in situ X-ray absorption and diffraction studies.[233] The origin of this crystallization mechanism lies in the formation of an intermediate, noncrystalline phase and in the time-dependent changes in the chemical environment. In spite of the commonly accepted polymorphic-crossover from anatase to rutile, triggered by the critical size of nanoparticles, the authors found that the respective nucleation and growth of rutile and anatase in solution were independent processes.

In addition to MoO_2 and TiO_2, also ZrO_2 shows varying phase composition in dependence of the reaction conditions. Garnweitner et al. presented a detailed mechanistic study on the fractal growth of ZrO_2 nanoparticles considering chemical as well as crystallization aspects. Systematic change of the precursor concentration and reaction temperature made it possible not only to tune the ratio of tetragonal-to-monoclinic zirconia, but also to grow either spherical or fractal morphologies.[158]

The solvent not only influences the crystal phase, but also the crystallinity. A comparison between benzyl alcohol and triethylene glycol (TEG) for the synthesis of magnetite/maghemite nanoparticles showed that at shorter reaction times the particles in benzyl alcohol were of much better crystallinity than those in TEG.[253] This observation is important for magnetic nanoparticles, because the magnetic properties are directly linked to the crystallinity. Indeed, the authors found a direct correlation of the crystallinity of the nanoparticles with their magnetic properties. Therefore, it was easily possible to obtain particles with a certain size, crystallinity and thus customized magnetic properties.[254] A follow-up study of the growth of iron oxide nanoparticles in TEG confirmed that in a first step an amorphous network was formed, which, upon expulsion of organic compounds, slowly crystallized and grew into hydrophilic iron oxide nanoparticles of about 8 nm in diameter.[255] Accordingly, particle formation in benzyl alcohol followed a classical nucleation and growth model, while in TEG a sol–gel reaction with an intermediate gel-like network occurred.

6. Surface Chemistry

After synthesis, the nanoparticles are typically present as powders, and for many applications these powders have to be further processed, for example, into films, composites or bulk structures. The processing often occurs in liquid medium, which means that the nanoparticles have to be redispersible in a solvent, and at that point, the surface chemistry of the nanoparticles plays a dominant role. First, one has to know, what is on the surface of the nanoparticles, and second, one has to be able to tune the surface chemistry according to the requirements for further processing of the nanoparticles.

The synthesis of metal oxide nanoparticles in organic solvents, with or without additional surfactants, always leads to organic residues attached to the surface. Accordingly, the metal oxide nanoparticles are, strictly spoken, organic-inorganic hybrid materials. The use of organic compounds to gain control over particle size and shape is meanwhile routine in nanoparticle synthesis. This strategy has been proven to be extremely successful, although the exact role of the organic species is often not fully understood. Another important task of the organic compounds during the synthesis is to prevent agglomeration of the nanoparticles and to facilitate their redispersion after synthesis. While surface-adsorbed organics are beneficial for nanoparticle processing, they are often detrimental for the final application, affecting the properties in a negative way. Based on all these considerations, three important research directions developed: i) Careful characterization of the surface-adsorbed species to understand their stabilizing effect, ii) efficient methods to remove or replace the surface-adsorbed species, and iii) exploitation of the chemistry of the surface-adsorbed species in catalysis and photocatalysis.

In the last few years, the importance of surface chemistry has been recognized. Surface-adsorbed organic, but also inorganic ligands have a tremendous effect on the nucleation and growth of the nanocrystals, on their chemical and physical properties (including dispersion and assembly behavior) and on their performance (e.g., as electrical conductors or as sensors).[256–259] For processing, and generally also for the final application of nanoparticles, the surface ligands have to be tuned to achieve high colloidal stability without aggregation of nanoparticles.[260] In this respect, surfactants, typically consisting of a coordinating head group and a long alkyl chain, bind to the nanoparticle surface during synthesis giving access to shape and size controlled nanocrystals with colloidal stability in nonpolar solvents.[15] Surfactant-free nonaqueous synthesis routes, on the other hand, usually result in agglomerated nanoparticles. In certain cases, however, the organic molecules from the solvent or from the reaction byproducts attached to the surface of the nanoparticles are sufficient to provide good dispersibility in organic solvents.[261–263] A particularly useful solvent in this regard is *tert*-butanol, which gave access to a wide variety of metal oxide nanoparticles with good dispersibility.[262,264–267] Another example is the nonhydrolytic reaction of metal chloride precursors with diisopropyl ether, yielding metal oxide nanoparticles coated by chloride and isopropoxide groups. Because of the unique surface chemistry, these nano-

particles were dispersible in organic solvents such as tetrahydrofuran (THF), and they were reactive towards water, alcohol or hydroxylated surfaces.[135,136,268]

If the as-synthesized nanoparticles are not dispersible, then a post-synthetic surface functionalization or ligand exchange is required. This strategy has the advantage that the optimum ligand for a specific application or processing step can be selected, independent of its compatibility with the synthesis protocol. For example, polymerizable vinyl-group containing ligands were used to functionalize zirconia nanoparticles[269] for their incorporation into polymers like poly(methyl methacrylate[270] or polyurethane.[271] A two-step modification approach involving silane chemistry was used to functionalize zirconia and alumina nanocrystals with carboxylic acids with a broad range of terminal functionalities.[272] Agglomerated indium tin oxide (ITO) nanoparticles, obtained by the benzyl alcohol route, were transformed into long-term stable dispersions in chloroform ($CHCl_3$) by stabilizing them by weakly coordinating ligands like primary unbranched alkylamines with different chain lengths.[273] In another study, a comparison of the post-synthetic stabilization of ITO and ZrO_2 nanoparticles with weakly and strongly coordinating ligands showed that for the ITO nanoparticles the weak and unspecific coordination of *n*-alkylamines led to stable nanoparticle dispersions in $CHCl_3$ (Figure 10, left), while the stabilization of ZrO_2 nanoparticles in the same solvent was achieved by addition of fatty acids through the selective binding of the carboxylate groups on the particle surface (Figure 10, right). Moreover, the stabilization of the ITO nanoparticles depended on the chain length and the amount of added stabilizer. In the case of ZrO_2 nanoparticles the influence of the stabilizer chain length was found to be much smaller.[88] The study also indicated that not only the adsorption of the ligand determined the stability of the dispersion, but also the desorption of organic residues from the synthesis.

De Roo et al. found that HfO_2 nanocrystals, synthesized by the solvothermal reaction of $HfCl_4$ with benzyl alcohol, could be transferred to nonpolar media using a mixture of carboxylic acids and amines.[274] Details of the transfer reaction and of the surface chemistry of the resulting sterically stabilized HfO_2 nanocrystals were revealed by solution ^1H NMR and IR spectroscopy. A model for the overall reaction during the surface modification is shown in Figure 11. The as-synthesized HfO_2 nanocrystals were charge stabilized by protons, with chlorides acting as the counterions. The carboxylic acid only bound to the nanoparticle surface in the presence of oleylamine. The oleylamine provided the basic environment for the dissociation of the carboxylic acid, which then replaced the chlorides, resulting in stable, aggregate-free dispersions. The authors obtained similar results with ZrO_2 nanocrystals.

A subsequent study analyzed the reversible ligand exchange of oleic acid molecules by octylamine and self-adsorption of oleic acid on the surface of HfO_2 nanocrystals using ^1H NMR and IR spectroscopy.[275] The Covalent Bond Classification (CBC), which provides an appropriate framework to describe the binding of ligands to the nanocrystal surface,[276] defines the ligands as L-, X-, or Z-type, depending on the number of electrons they contribute to the nanocrystal-ligand bond (2, 1, or 0, respectively). L-type ligands such as amines are neutral donors of a free electron pair. The dissociative adsorption of carboxylic acids brings two X-type ligands to the nanocrystal surface, namely a carboxylate and a proton, yielding a combined charge-neutral X_2 binding motif, which allows for self-adsorption (Figure 12 B) and exchange for L-type ligands (Fig-

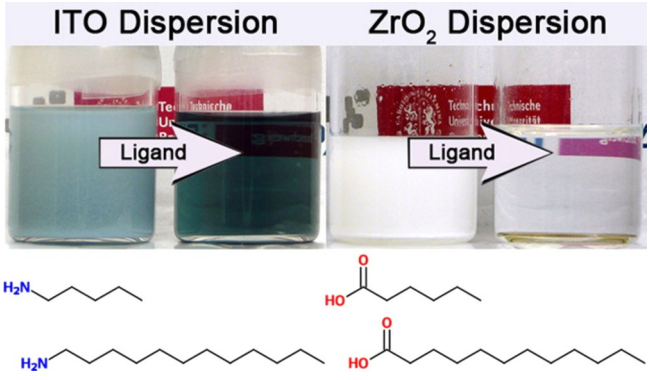

Figure 10. Photographs of ITO and ZrO_2 nanoparticle dispersions in $CHCl_3$ before and after the postsynthetic stabilization with dodecylamine (ITO) and n-decanoic acid (ZrO_2). Reprinted with permission from ref. [88]. Copyright (2012) American Chemical Society.

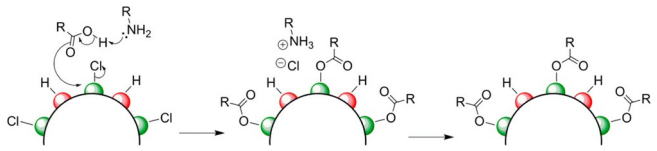

Figure 11. Schematic of the surface modification of HCl-terminated nanocrystals. The amine captures a proton of the carboxylic acid, which subsequently replaces the chloride. The chloride forms an ammonium salt and remains in the ligand shell. The nanocrystals are purified (precipitated and redispersed) with polar solvents to remove the salt from the ligand shell. The final result is a dissociated carboxylic acid on the surface of HfO_2 or ZrO_2 nanoparticles. Reprinted with permission from ref. [274]. Copyright (2014) American Chemical Society.

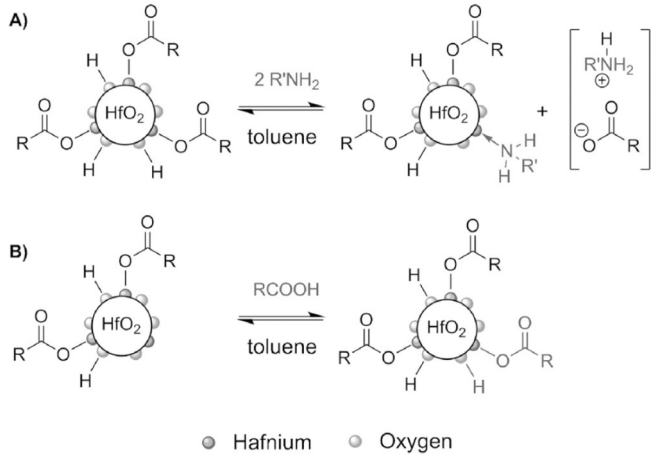

Figure 12. Schematic of A) the substitution of an X_2-type carboxylic acid by an L-type alkylamine, and B) autoadsorption of a carboxylic acid onto the surface of a HfO_2 nanocrystal. Scheme reproduced from ref. [275].

ure 12 A). The displacement of dissociated carboxylic acids (charge-neutral X_2 motif) from the surface by L-type alkylamines is driven by ion-pair formation as shown in Figure 12 A.

The nonaqueous synthesis of water dispersible metal oxide nanoparticles is clearly a challenge. One possibility is to add polar stabilizers to the initial reaction mixture,[141,277] another one the substitution of the surfactant by a more polar ligand in a postsynthetic treatment. De Roo et al. studied the mechanism of amino acid based ligand exchange reactions for the phase transfer of carboxylic acid capped HfO_2 and ZrO_2 nanocrystals to various polar solvents using a combination of FTIR, zeta potential measurements, and ^{1}H NMR techniques.[278] They found that a strong acid was necessary to protonate the original carboxylic acid ligand at the nanocrystal surface, after which a positively charged amino acid bound to the surface, stabilizing the dispersion electrostatically. However, a small amount of remaining carboxylic acid provided an additional steric contribution to the colloidal stabilization.

For a more exhaustive overview of the chemical principles behind surface ligation and ligand exchange reactions as well as for a detailed discussion of the different binding motifs, the reader is referred to more dedicated review articles.[279,280]

In addition to the nanoparticle surface-solvent bonding, also the interactions of the surfactant molecules with the solvent play an important role in tuning the dispersibility of nanoparticles in organic solvents. Leite and co-workers investigated the dispersibility behavior of antimony doped tin oxide (ATO) nanocrystals in THF and $CHCl_3$ in the presence of oleic acid and oleylamine.[281] They found that the combination of THF/oleylamine or $CHCl_3$/oleylamine was very effective in obtaining colloidally stable ATO nanocrystals in a high concentration, while oleic acid did not promote the dispersibility in the same solvents. Based on a set of molecular dynamics simulations of oleic acid and oleylamine in both $CHCl_3$ and THF, it was found that the oleic acid in chlorofom favored the formation of oleic acid dimers, and in THF it formed stable oleic acid-solvent pairs. In both cases the association of oleic acid molecules via hydrogen bonds strongly decreased its effectiveness as a surfactant to stabilize metal oxide nanoparticles in comparison to oleylamine, which is essentially free in $CHCl_3$ and THF and available for coordination to the nanoparticles.

7. Conclusion

Nanoparticle research is a mature and well established research field. An immense number of synthesis protocols gave access to a wide variety of nanomaterials with a broad range of properties. But in spite of all this progress, two major issues are not yet satisfactorily solved: Detailed mechanistic understanding of the chemical and crystallization processes taking place in a specific reaction system, and in-depth knowledge about the surface properties of nanoparticles. Mechanistic know-how is essential for a rational synthesis design, and surface chemistry is crucial for nanoparticle processing and their performance in many applications. Nevertheless, synthesis development as well as surface functionalization work extremely well, however, mainly based on empirical know-how of the different research groups. There is no doubt that generally applicable guidelines and principles would tremendously accelerate the progress in the field.

In this review we provided an overview of chemical formation and crystallization mechanisms occurring in nonaqueous/nonhydrolytic sol–gel routes to metal oxide nanoparticles. This synthesis method has rapidly developed in the last decade and considerable understanding of chemical formation and crystallization mechanisms has accumulated, mainly due to the availability of new and powerful characterization tools especially for in situ studies.

The mechanistic part of the review is structured according to the most frequently applied precursor-solvent systems. This systematic structure helps the reader to quickly find the relevant information for a specific synthesis mixture (without necessarily reading the whole review article). Nevertheless, we tried to elaborate the similarities, but also the differences, between the systems to provide an integral and overall picture of the various nonaqueous routes, including advantages and limitations. The idea is to offer assistance for selecting the appropriate reaction system for the synthesis of specific metal oxide nanoparticles.

We also included a section on crystallization mechanisms. We believe that this is an important aspect, because nucleation and growth, and thus nanoparticle size, shape and crystal structure are strongly determined by the precursor-solvent system. Accordingly, for a rational synthesis planning it is important to include considerations regarding crystallization pathways.

The last section is dedicated to the surface chemistry. Nonaqueous routes always lead to organic residues attached to the surface of the inorganic nanoparticles. These organic compounds may be or may be not beneficial for the properties of the nanoparticles. But in any case, it is important to know, what is on the surface. In this regard, surface chemistry and chemical formation mechanisms are strongly interlinked, because organic species formed in situ during nanoparticle formation have to be taken into account, and this is only possible, if the chemical formation mechanism is known.

Acknowledgement

We thank ETH Zurich and the Swiss National Science Foundation (project no. 20PC21_155658) for financial support.

Conflict of interest

The authors declare no conflict of interest.

Keywords: nanoparticles · oxides · reaction mechanisms · sol–gel processes · surface chemistry

[1] M. Niederberger, G. Garnweitner, *Chem. Eur. J.* **2006**, *12*, 7282.
[2] A. I. Hochbaum, P. Yang, *Chem. Rev.* **2010**, *110*, 527.
[3] Q. Zhang, E. Uchaker, S. L. Candelaria, G. Cao, *Chem. Soc. Rev.* **2013**, *42*, 3127.

[4] P. Trogadas, V. Ramani, P. Strasser, T. F. Fuller, M.-O. Coppens, *Angew. Chem. Int. Ed.* **2016**, *55*, 122; *Angew. Chem.* **2016**, *128*, 128.
[5] P. G. Bruce, B. Scrosati, J.-M. Tarascon, *Angew. Chem. Int. Ed.* **2008**, *47*, 2930; *Angew. Chem.* **2008**, *120*, 2972.
[6] F. Zaera, *Chem. Soc. Rev.* **2013**, *42*, 2746.
[7] S. Schauermann, N. Nilius, S. Shaikhutdinov, H.-J. Freund, *Acc. Chem. Res.* **2013**, *46*, 1673.
[8] J. Pal, T. Pal, *Nanoscale* **2015**, *7*, 14159.
[9] B. D. Terris, T. Thomson, *J. Phys. D Appl. Phys.* **2005**, *38*, R199.
[10] N. Sanvicens, M. P. Marco, *Trends Biotechnol.* **2008**, *26*, 425.
[11] J. Gao, H. Gu, B. Xu, *Acc. Chem. Res.* **2009**, *42*, 1097.
[12] D. A. Giljohann, D. S. Seferos, W. L. Daniel, M. D. Massich, P. C. Patel, C. A. Mirkin, *Angew. Chem. Int. Ed.* **2010**, *49*, 3280; *Angew. Chem.* **2010**, *122*, 3352.
[13] W. J. Stark, P. R. Stoessel, W. Wohlleben, A. Hafner, *Chem. Soc. Rev.* **2015**, *44*, 5793.
[14] C. Burda, X. B. Chen, R. Narayanan, M. A. El-Sayed, *Chem. Rev.* **2005**, *105*, 1025.
[15] J. Chang, E. R. Waclawik, *RSC Adv.* **2014**, *4*, 23505.
[16] S. Diodati, P. Dolcet, M. Casarin, S. Gross, *Chem. Rev.* **2015**, *115*, 11449.
[17] A. E. Danks, S. R. Hall, Z. Schnepp, *Mater. Horiz.* **2016**, *3*, 91.
[18] H. Dong, Y. C. Chen, C. Feldmann, *Green Chem.* **2015**, *17*, 4107.
[19] J. van Embden, A. S. R. Chesman, J. J. Jasieniak, *Chem. Mater.* **2015**, *27*, 2246.
[20] R. Strobel, S. E. Pratsinis, *J. Mater. Chem.* **2007**, *17*, 4743.
[21] W. Y. Teoh, R. Amal, L. Maedler, *Nanoscale* **2010**, *2*, 1324.
[22] A. Glasner, *Mater. Res. Bull.* **1973**, *8*, 413.
[23] J. J. De Yoreo, P. U. P. A. Gilbert, N. A. J. M. Sommerdijk, R. L. Penn, S. Whitelam, D. Joester, H. Zhang, J. D. Rimer, A. Navrotsky, J. F. Banfield, A. F. Wallace, F. M. Michel, F. C. Meldrum, H. Coelfen, P. M. Dove, *Science* **2015**, *349*, 498.
[24] D. Gebauer, M. Kellermeier, J. D. Gale, L. Bergstrom, H. Coelfen, *Chem. Soc. Rev.* **2014**, *43*, 2348.
[25] Q. Zhang, S.-J. Liu, S.-H. Yu, *J. Mater. Chem.* **2009**, *19*, 191.
[26] R. L. Penn, J. A. Soltis, *Crystengcomm* **2014**, *16*, 1409.
[27] M. Niederberger, H. Coelfen, *Phys. Chem. Chem. Phys.* **2006**, *8*, 3271.
[28] H. Cölfen, M. Antonietti, *Angew. Chem. Int. Ed.* **2005**, *44*, 5576; *Angew. Chem.* **2005**, *117*, 5714.
[29] D. Koziej, *Chem. Mater.* **2016**, *28*, 2478.
[30] J.-D. Grunwaldt, C. G. Schroer, *Chem. Soc. Rev.* **2010**, *39*, 4741.
[31] J. D. Grunwaldt, M. Ramin, M. Rohr, A. Michailovski, G. R. Patzke, A. Baiker, *Rev. Sci. Instrum.* **2005**, *76*, 054104.
[32] S. R. Bare, N. Yang, S. D. Kelly, G. E. Mickelson, F. S. Modica, *Catal. Today* **2007**, *126*, 18.
[33] M. Staniuk, O. Hirsch, N. Kraenzlin, R. Boehlen, W. van Beek, P. M. Abdala, D. Koziej, *Chem. Mater.* **2014**, *26*, 2086.
[34] R. Deshmukh, M. Niederberger, in *The Sol–gel Handbook*, Vol. 1 (Eds: D. Levy, M. Zayat), Wiley-VCH, Weinheim 2015.
[35] M. Niederberger, N. Pinna, *Metal Oxide Nanoparticles in Organic Solvents: Synthesis Formation, Assembly and Applications*, Springer, Heidelberg, **2009**.
[36] P. H. Mutin, A. Vioux, *Chem. Mater.* **2009**, *21*, 582.
[37] P. H. Mutin, A. Vioux, *J. Mater. Chem. A* **2013**, *1*, 11504.
[38] D. P. Debecker, P. H. Mutin, *Chem. Soc. Rev.* **2012**, *41*, 3624.
[39] N. Pinna, M. Niederberger, *Angew. Chem. Int. Ed.* **2008**, *47*, 5292; *Angew. Chem.* **2008**, *120*, 5372.
[40] B. Ludi, I. Olliges-Stadler, M. D. Rossell, M. Niederberger, *Chem. Commun.* **2011**, *47*, 5280.
[41] S. Sallard, E. Castel, C. Villevieille, P. Novak, *J. Mater. Chem. A* **2015**, *3*, 16112.
[42] R. Deshmukh, G. Zeng, E. Tervoort, M. Staniuk, D. Wood, M. Niederberger, *Chem. Mater.* **2015**, *27*, 8282.
[43] F. J. Heiligtag, M. Niederberger, *Mater Today* **2013**, *16*, 262.
[44] M. Niederberger, *Acc. Chem. Res.* **2007**, *40*, 793.
[45] G. Garnweitner, M. Niederberger, *J. Mater. Chem.* **2008**, *18*, 1171.
[46] N. Pinna, G. Garnweitner, P. Beato, M. Niederberger, M. Antonietti, *Small* **2005**, *1*, 112.
[47] I. Olliges-Stadler, M. D. Rossell, M. Niederberger, *Small* **2010**, *6*, 960.
[48] N. Pinna, *J. Mater. Chem.* **2007**, *17*, 2769.
[49] M. Karmaoui, R. A. S. Ferreira, A. T. Mane, L. D. Carlos, N. Pinna, *Chem. Mater.* **2006**, *18*, 4493.
[50] M. H. Cao, I. Djerdj, Z. Jaglicic, M. Antonietti, M. Niederberger, *Phys. Chem. Chem. Phys.* **2009**, *11*, 6166.
[51] I. Djerdj, M. H. Cao, X. Rocquefelte, R. Cerny, Z. Jaglicic, D. Arcon, A. Potocnik, F. Gozzo, M. Niederberger, *Chem. Mater.* **2009**, *21*, 3356.
[52] N. Y. Turova, E. P. Turevskaya, V. G. Kessler, M. I. Yanovskaya, *The Chemistry of Metal Alkoxides*, Kluwer Academic Publishers, Massachusetts **2002**.
[53] D. Bradley, R. C. Mehrotra, I. Rothwell, *Alkoxo and Aryloxo Derivatives of Metals*, Academic Press, London, **2001**.
[54] R. J. P. Corriu, D. Leclercq, P. Lefevre, P. H. Mutin, A. Vioux, *J. Non-Cryst. Solids* **1992**, *146*, 301.
[55] R. J. P. Corriu, D. Leclercq, P. Lefevre, P. H. Mutin, A. Vioux, *J. Mater. Chem.* **1992**, *2*, 673.
[56] R. Corriu, D. Leclercq, P. Lefevre, P. H. Mutin, A. Vioux, *Chem. Mater.* **1992**, *4*, 961.
[57] M. Niederberger, G. Garnweitner, N. Pinna, M. Antonietti, *J. Am. Chem. Soc.* **2004**, *126*, 9120.
[58] A. Vioux, *Chem. Mater.* **1997**, *9*, 2292.
[59] G. Garnweitner, M. Niederberger in *Advanced Wet-Chemical Synthetic Approaches to Inorganic Nanostructures* (Ed.: P. D. Cozzoli), Transworld Research Network, Kerala, **2008**.
[60] M. Fernández-García, A. Martinez-Arias, J. C. Hanson, J. A. Rodriguez, *Chem. Rev.* **2004**, *104*, 4063.
[61] B. M. Weckhuysen, *Chem. Soc. Rev.* **2010**, *39*, 4557.
[62] A. P. Alivisatos, *J. Phys. Chem.* **1996**, *100*, 13226.
[63] M. A. El-Sayed, *Acc. Chem. Res.* **2004**, *37*, 326.
[64] A. G. Vega-Poot, G. Rodriguez-Gattorno, O. E. Soberanis-Dominguez, R. T. Patino-Diaz, M. Espinosa-Pesqueira, G. Oskam, *Nanoscale* **2010**, *2*, 2710.
[65] R. Viswanatha, P. K. Santra, C. Dasgupta, D. D. Sarma, *Phys. Rev. Lett.* **2007**, *98*, 255501.
[66] C. Lizandara-Pueyo, M. W. E. van den Berg, A. De Toni, T. Goes, S. Polarz, *J. Am. Chem. Soc.* **2008**, *130*, 16601.
[67] V. Briois, C. Giorgetti, F. Baudelet, S. Blanchandin, M. S. Tokumoto, S. H. Pulcinelli, C. V. Santilli, *J. Phys. Chem. C* **2007**, *111*, 3253.
[68] B. Ludi, M. Niederberger, *Dalton Trans.* **2013**, *42*, 12554.
[69] R. A. Schoonheydt, *Chem. Soc. Rev.* **2010**, *39*, 5051.
[70] B. L. Mojet, S. D. Ebbesen, L. Lefferts, *Chem. Soc. Rev.* **2010**, *39*, 4643.
[71] J. Jaumot, R. Gargallo, A. de Juan, R. Tauler, *Chemom. Intell. Lab. Syst.* **2005**, *76*, 101.
[72] J. Felten, H. Hall, J. Jaumot, R. Tauler, A. de Juan, A. Gorzsas, *Nat. Protoc.* **2015**, *10*, 217.
[73] J.-M. Andanson, A. Baiker, *Chem. Soc. Rev.* **2010**, *39*, 4571.
[74] A. R. Hind, S. K. Bhargava, A. McKinnon, *Adv. Colloid Interface Sci.* **2001**, *93*, 91.
[75] A. J. McQuillan, *Adv. Mater.* **2001**, *13*, 1034.
[76] G. Garnweitner, C. Grote, *Phys. Chem. Chem. Phys.* **2009**, *11*, 3767.
[77] M. Staniuk, D. Zindel, W. van Beek, O. Hirsch, N. Kraenzlin, M. Niederberger, D. Koziej, *Crystengcomm* **2015**, *17*, 6962.
[78] S. Gross, M. Bauer, *Adv. Funct. Mater.* **2010**, *20*, 4026.
[79] A. K. Cheetham, C. F. Mellot, *Chem. Mater.* **1997**, *9*, 2269.
[80] A. Michailovski, J. D. Grunwaldt, A. Baiker, R. Kiebach, W. Bensch, G. R. Patzke, *Angew. Chem. Int. Ed.* **2005**, *44*, 5643; *Angew. Chem.* **2005**, *117*, 5787.
[81] D. Koziej, M. D. Rossell, B. Ludi, A. Hintennach, P. Novak, J.-D. Grunwaldt, M. Niederberger, *Small* **2011**, *7*, 377.
[82] T. Blasco, *Chem. Soc. Rev.* **2010**, *39*, 4685.
[83] C. E. Hughes, K. D. M. Harris, *J. Phys. Chem. A* **2008**, *112*, 6808.
[84] C. E. Hughes, P. A. Williams, K. D. M. Harris, *Angew. Chem. Int. Ed.* **2014**, *53*, 8939; *Angew. Chem.* **2014**, *126*, 9085.
[85] N. Pienack, W. Bensch, *Angew. Chem. Int. Ed.* **2011**, *50*, 2014; *Angew. Chem.* **2011**, *123*, 2062.
[86] N. Pinna, G. Garnweitner, M. Antonietti, M. Niederberger, *Adv. Mater.* **2004**, *16*, 2196.
[87] Z. Hens, J. C. Martins, *Chem. Mater.* **2013**, *25*, 1211.
[88] C. Grote, T. A. Cheema, G. Garnweitner, *Langmuir* **2012**, *28*, 14395.
[89] J. De Roo, I. Van Driessche, J. C. Martins, Z. Hens, *Nat. Mater.* **2016**, *15*, 517.
[90] R. I. Walton, D. O'Hare, *Chem. Commun.* **2000**, 2283.
[91] K. M. O. Jensen, C. Tyrsted, M. Bremholm, B. B. Iversen, *Chemsuschem* **2014**, *7*, 1594.

[92] M. J. Geselbracht, R. I. Walton, E. S. Cowell, F. Millange, D. O'Hare, *Rev. Sci. Instrum.* **2000**, *71*, 4177.
[93] C. Tyrsted, K. M. O. Jensen, E. D. Bojesen, N. Lock, M. Christensen, S. J. L. Billinge, B. B. Iversen, *Angew. Chem. Int. Ed.* **2012**, *51*, 9030; *Angew. Chem.* **2012**, *124*, 9164.
[94] C. Tyrsted, B. R. Pauw, K. M. O. Jensen, J. Becker, M. Christensen, B. B. Iversen, *Chem. Eur. J.* **2012**, *18*, 5759.
[95] K. M. O. Jensen, M. Christensen, P. Juhas, C. Tyrsted, E. D. Bojesen, N. Lock, S. J. L. Billinge, B. B. Iversen, *J. Am. Chem. Soc.* **2012**, *134*, 6785.
[96] K. M. O. Jensen, H. L. Andersen, C. Tyrsted, E. D. Bojesen, A. C. Dippel, N. Lock, S. J. L. Billinge, B. B. Iversen, M. Christensen, *ACS Nano* **2014**, *8*, 10704.
[97] D. Saha, K. M. O. Jensen, C. Tyrsted, E. D. Bojesen, A. H. Mamakhel, A. C. Dippel, M. Christensen, B. B. Iversen, *Angew. Chem. Int. Ed.* **2014**, *53*, 3667; *Angew. Chem.* **2014**, *126*, 3741.
[98] J. Munn, P. Barnes, D. Hausermann, S. A. Axon, J. Klinowski, *Phase Transitions* **1992**, *39*, 129.
[99] R. J. Francis, S. O'Brien, A. M. Fogg, P. S. Halasyamani, D. O'Hare, T. Loiseau, G. Ferey, *J. Am. Chem. Soc.* **1999**, *121*, 1002.
[100] S. O'Brien, R. J. Francis, A. Fogg, D. O'Hare, N. Okazaki, K. Kuroda, *Chem. Mater.* **1999**, *11*, 1822.
[101] N. Kränzlin, S. Ellenbroek, D. Duran-Martin, M. Niederberger, *Angew. Chem. Int. Ed.* **2012**, *51*, 4743; *Angew. Chem.* **2012**, *124*, 4824.
[102] N. Kränzlin, W. van Beek, M. Niederberger, D. Koziej, *Adv. Mater. Interfaces* **2015**, *2*, 1500094.
[103] B. Chu, B. S. Hsiao, *Chem. Rev.* **2001**, *101*, 1727.
[104] C. E. Blanchet, D. I. Svergun, *Annu. Rev. Phys. Chem.* **2013**, *64*, 37.
[105] S. Skou, R. E. Gillilan, N. Ando, *Nat. Protoc.* **2014**, *9*, 1727.
[106] I. Olliges-Stadler, M. D. Rossell, M. J. Sueess, B. Ludi, O. Bunk, J. S. Pedersen, H. Birkedal, M. Niederberger, *Nanoscale* **2013**, *5*, 8517.
[107] M. D. Rossell, Q. M. Ramasse, S. D. Findlay, F. Rechberger, R. Erni, M. Niederberger, *ACS Nano* **2012**, *6*, 7077.
[108] N. de Jonge, F. M. Ross, *Nat. Nanotechnol.* **2011**, *6*, 695.
[109] J. Meurig Thomas, P. A. Midgley, *Chem. Commun.* **2004**, 1253.
[110] S. Carenco, S. Moldovan, L. Roiban, I. Florea, D. Portehault, K. Valle, P. Belleville, C. Boissiere, L. Rozes, N. Mezailles, M. Drillon, C. Sanchez, O. Ersen, *Nanoscale* **2016**, *8*, 1260.
[111] N. Ravishankar, *J. Phys. Chem. Lett.* **2010**, *1*, 1212.
[112] H. Zheng, R. K. Smith, Y.-w. Jun, C. Kisielowski, U. Dahmen, A. P. Alivisatos, *Science* **2009**, *324*, 1309.
[113] J. M. Yuk, J. Park, P. Ercius, K. Kim, D. J. Hellebusch, M. F. Crommie, J. Y. Lee, A. Zettl, A. P. Alivisatos, *Science* **2012**, *336*, 61.
[114] D. Li, M. H. Nielsen, J. R. I. Lee, C. Frandsen, J. F. Banfield, J. J. De Yoreo, *Science* **2012**, *336*, 1014.
[115] H.-G. Liao, L. Cui, S. Whitelam, H. Zheng, *Science* **2012**, *336*, 1011.
[116] X. Chen, C. Li, H. Cao, *Nanoscale* **2015**, *7*, 4811.
[117] K. De Keukeleere, J. De Roo, P. Lommens, J. C. Martins, P. Van der Voort, I. Van Driessche, *Inorg. Chem.* **2015**, *54*, 3469.
[118] G. A. Seisenbaeva, V. G. Kessler, *Nanoscale* **2014**, *6*, 6229.
[119] Z. H. Wu, S. L. Yang, W. Wu, *Nanoscale* **2016**, *8*, 1237.
[120] T. D. Nguyen, *Nanoscale* **2013**, *5*, 9455.
[121] J. Park, J. Joo, S. G. Kwon, Y. Jang, T. Hyeon, *Angew. Chem. Int. Ed.* **2007**, *46*, 4630; *Angew. Chem.* **2007**, *119*, 4714.
[122] M. Zimmermann, K. Ibrom, P. G. Jones, G. Garnweitner, *ChemNanoMat* **2016**, *2*, 1073.
[123] S. Acosta, R. J. P. Corriu, D. Leclercq, P. Lefevre, P. H. Mutin, A. Vioux, *J. Non-Cryst. Solids* **1994**, *170*, 234.
[124] L. Bourget, R. J. P. Corriu, D. Leclercq, P. H. Mutin, A. Vioux, *J. Non-Cryst. Solids* **1998**, *242*, 81.
[125] T. J. Trentler, T. E. Denler, J. F. Bertone, A. Agrawal, V. L. Colvin, *J. Am. Chem. Soc.* **1999**, *121*, 1613.
[126] P. Arnal, R. J. P. Corriu, D. Leclercq, P. H. Mutin, A. Vioux, *Chem. Mater.* **1997**, *9*, 694.
[127] J. Joo, T. Yu, Y. W. Kim, H. M. Park, F. X. Wu, J. Z. Zhang, T. Hyeon, *J. Am. Chem. Soc.* **2003**, *125*, 6553.
[128] J. Tang, J. Fabbri, R. D. Robinson, Y. M. Zhu, I. P. Herman, M. L. Steigerwald, L. E. Brus, *Chem. Mater.* **2004**, *16*, 1336.
[129] M. Ritala, K. Kukli, A. Rahtu, P. I. Raisanen, M. Leskela, T. Sajavaara, J. Keinonen, *Science* **2000**, *288*, 319.
[130] W. K. Kim, S. W. Kang, S. W. Rhee, *J. Vac. Sci. Technol. A* **2003**, *21*, L16.
[131] V. V. Brei, V. A. Kaspersky, N. U. Gulyanitskaya, *React. Kinet. Catal. Lett.* **1993**, *50*, 415.
[132] A. Rahtu, M. Ritala, *Langmuir* **2002**, *18*, 10046.
[133] V. R. Anderson, A. S. Cavanagh, A. I. Abdulagatov, Z. M. Gibbs, S. M. George, *J. Vac. Sci. Technol. A* **2014**, *32*, 01A114.
[134] M. Niederberger, M. H. Bartl, G. D. Stucky, *J. Am. Chem. Soc.* **2002**, *124*, 13642.
[135] A. Aboulaich, B. Boury, P. H. Mutin, *Chem. Mater.* **2010**, *22*, 4519.
[136] A. Aboulaich, O. Lorret, B. Boury, P. H. Mutin, *Chem. Mater.* **2009**, *21*, 2577.
[137] D. Portehault, C. Giordano, C. Sanchez, M. Antonietti, *Chem. Mater.* **2010**, *22*, 2125.
[138] J. G. Wang, F. L. Cao, Z. F. Bian, M. K. H. Leung, H. X. Li, *Nanoscale* **2014**, *6*, 897.
[139] S. Pokhrel, C. E. Simion, V. S. Teodorescu, N. Barsan, U. Weimar, *Adv. Funct. Mater.* **2009**, *19*, 1767.
[140] L. H. Tian, J. Y. Liu, C. Q. Gong, L. Q. Ye, L. Zan, *J. Nanopart. Res.* **2013**, *15*, 1917.
[141] G. Garnweitner, H. O. Ghareeb, C. Grote, *Colloids Surf. A* **2010**, *372*, 41.
[142] M. J. Hu, J. F. Gao, S. L. Yang, Y. C. Dong, J. S. P. Wong, J. J. Xu, G. C. Shan, R. K. Y. Li, *Nanoscale* **2012**, *4*, 6284.
[143] M. J. Hu, J. J. Xu, J. F. Gao, S. L. Yang, J. S. P. Wong, R. K. Y. Li, *Dalton Trans.* **2013**, *42*, 9777.
[144] F. B. F. Silva, E. C. Paris, G. M. da Costa, C. Ribeiro, *RSC Adv.* **2014**, *4*, 53265.
[145] W. Gerrard, A. H. Woodhead, *J. Chem. Soc.* **1951**, 519.
[146] J. A. Zhu, S. H. Wang, Z. F. Bian, S. H. Xie, C. L. Cai, J. G. Wang, H. G. Yang, H. X. Li, *Crystengcomm* **2010**, *12*, 2219.
[147] D. Morselli, M. Niederberger, I. Bilecka, F. Bondioli, *J. Nanopart. Res.* **2014**, *16*, 2645.
[148] I. Olliges-Stadler, J. Stoetzel, D. Koziej, M. D. Rossell, J.-D. Grunwaldt, M. Nachtegaal, R. Frahm, M. Niederberger, *Chem. Eur. J.* **2012**, *18*, 2305.
[149] E. Ohayon, A. Gedanken, *Ultrason. Sonochem.* **2010**, *17*, 173.
[150] D. C. Bradley, B. N. Chakravarti, W. Wardlaw, *J. Chem. Soc.* **1956**, 2381.
[151] D. C. Bradley, B. N. Chakravarti, W. Wardlaw, *J. Chem. Soc.* **1956**, 4439.
[152] N. Y. Turova, V. G. Kessler, S. I. Kucheiko, *Polyhedron* **1991**, *10*, 2617.
[153] V. G. Kessler, K. V. Nikitin, A. I. Belokon, *Polyhedron* **1998**, *17*, 2309.
[154] R. Pazik, R. Tekoriute, S. Hakansson, R. Wiglusz, W. Strek, G. A. Seisenbaeva, Y. K. Gun'ko, V. G. Kessler, *Chem. Eur. J.* **2009**, *15*, 6820.
[155] M. Inoue, H. Kominami, T. Inui, *Appl. Catal. A* **1993**, *97*, L25.
[156] G. Garnweitner, L. M. Goldenberg, O. V. Sakhno, M. Antonietti, M. Niederberger, J. Stumpe, *Small* **2007**, *3*, 1626.
[157] M. Karmaoui, D. M. Tobaldi, A. S. Skapin, R. C. Pullar, M. P. Seabra, J. A. Labrincha, V. S. Amaral, *RSC Adv.* **2014**, *4*, 46762.
[158] P. Stolzenburg, A. Freytag, N. C. Bigall, G. Garnweitner, *Crystengcomm* **2016**, *18*, 8396.
[159] M. Zimmermann, G. Garnweitner, *Crystengcomm* **2012**, *14*, 8562.
[160] R. Zhang, S. Santangelo, E. Fazio, F. Neri, M. D'Arienzo, F. Morazzoni, Y. H. Zhang, N. Pinna, P. A. Russo, *Chem. Eur. J.* **2015**, *21*, 14901.
[161] N. Le Houx, G. Pourroy, F. Camerel, M. Comet, D. Spitzer, *J. Phys. Chem. C* **2010**, *114*, 155.
[162] F. Böttger-Hiller, R. Lungwitz, A. Seifert, M. Hietschold, M. Schlesinger, M. Mehring, S. Spange, *Angew. Chem. Int. Ed.* **2009**, *48*, 8878; *Angew. Chem.* **2009**, *121*, 9039.
[163] A. Braendle, A. Perevedentsev, N. J. Cheetham, P. N. Stavrinou, J. A. Schachner, N. C. Mösch-Zanetti, M. Niederberger, W. R. Caseri, *J. Polym. Sci. Pol. Phys.* **2017**, *55*, 707.
[164] J. De Roo, K. De Keukeleere, J. Feys, P. Lommens, Z. Hens, I. Van Driessche, *J. Nanopart. Res.* **2013**, *15*, 1778.
[165] S. A. Veldhuis, W. J. C. Vijselaar, T. M. Stawski, J. E. ten Elshof, *Inorg. Chem.* **2014**, *53*, 13188.
[166] E. G. S. Firmiano, M. A. L. Cordeiro, A. C. Rabelo, C. J. Dalmaschio, A. N. Pinheiro, E. C. Pereira, E. R. Leite, *Chem. Commun.* **2012**, *48*, 7687.
[167] N. Pinna, G. Garnweitner, M. Antonietti, M. Niederberger, *J. Am. Chem. Soc.* **2005**, *127*, 5608.
[168] G. Garnweitner, N. Tsedev, H. Dierke, M. Niederberger, *Eur. J. Inorg. Chem.* **2008**, 890.
[169] N. Pinna, S. Grancharov, P. Beato, P. Bonville, M. Antonietti, M. Niederberger, *Chem. Mater.* **2005**, *17*, 3044.
[170] B. Ludi, M. J. Sueess, I. A. Werner, M. Niederberger, *Nanoscale* **2012**, *4*, 1982.

[171] L. Cigarini, D. Vanossi, F. Bondioli, C. Fontanesi, *Phys. Chem. Chem. Phys.* **2015**, *17*, 20522.
[172] D. Visinescu, M. Scurtu, R. Negrea, R. Birjega, D. C. Culita, M. C. Chifiriuc, C. Draghici, J. C. Moreno, A. M. Musuc, I. Balint, O. Carp, *RSC Adv.* **2015**, *5*, 99976.
[173] G. Ambrozic, S. D. Skapin, M. Zigon, Z. C. Orel, *J. Colloid Interface Sci.* **2010**, *346*, 317.
[174] H. Damm, A. Kelchtermans, A. Bertha, F. Van den Broeck, K. Elen, J. C. Martins, R. Carleer, J. D'Haen, C. De Dobbelaere, J. Hadermann, A. Hardy, M. K. Van Bael, *RSC Adv.* **2013**, *3*, 23745.
[175] L. Z. Zhang, G. Garnweitner, I. Djerdj, M. Antonietti, M. Niederberger, *Chem. Asian J.* **2008**, *3*, 746.
[176] A. Singhal, B. Sanyal, A. K. Tyagi, *RSC Adv.* **2011**, *1*, 903.
[177] M. Cao, I. Djerdj, M. Antonietti, M. Niederberger, *Chem. Mater.* **2007**, *19*, 5830.
[178] M. Karmaoui, S. G. Leonardi, D. M. Tobaldi, N. Donato, R. C. Pullar, M. P. Seabra, J. A. Labrincha, G. Neri, *J. Mater. Chem. B* **2015**, *3*, 399.
[179] S. X. Zhou, M. Antonietti, M. Niederberger, *Small* **2007**, *3*, 763.
[180] W. S. Seo, H. H. Jo, K. Lee, B. Kim, S. J. Oh, J. T. Park, *Angew. Chem. Int. Ed.* **2004**, *43*, 1115; *Angew. Chem.* **2004**, *116*, 1135.
[181] W. S. Seo, H. H. Jo, K. Lee, J. T. Park, *Adv. Mater.* **2003**, *15*, 795.
[182] J. Caruso, M. J. Hampdensmith, E. N. Duesler, *J. Chem. Soc. Chem. Commun.* **1995**, 1041.
[183] O. Igbari, Y. M. Xie, Z. M. Jin, L. S. Liao, *J. Alloys Compd.* **2015**, *653*, 219.
[184] G. Melcarne, L. De Marco, E. Carlino, F. Martina, M. Manca, R. Cingolani, G. Gigli, G. Ciccarella, *J. Mater. Chem.* **2010**, *20*, 7248.
[185] K. C. Pande, R. C. Mehrotra, *Z. Anorg. Allg. Chem.* **1957**, *290*, 95.
[186] I. Bilecka, P. Elser, M. Niederberger, *ACS Nano* **2009**, *3*, 467.
[187] M. Ivanda, S. Music, S. Popovic, M. Gotic, *J. Mol. Struct.* **1999**, *481*, 645.
[188] L. Wahba, M. D'Arienzo, S. Dire, R. Donetti, T. Hanel, F. Morazzoni, M. Niederberger, N. Santo, L. Tadiello, R. Scotti, *Soft Matter* **2014**, *10*, 2234.
[189] J. Caruso, M. J. Hampden-Smith, *J. Sol–gel Sci. Technol.* **1997**, *8*, 35.
[190] C. Wang, Z. X. Deng, Y. D. Li, *Inorg. Chem.* **2001**, *40*, 5210.
[191] M. Jansen, E. Guenther, *Chem. Mater.* **1995**, *7*, 2110.
[192] A. Styskalik, D. Skoda, J. Pinkas, S. Mathur, *J. Sol–gel Sci. Technol.* **2012**, *63*, 463.
[193] J. Joo, S. G. Kwon, T. Yu, M. Cho, J. Lee, J. Yoon, T. Hyeon, *J. Phys. Chem. B* **2005**, *109*, 15297.
[194] K. G. Sharp, *J. Sol–gel Sci. Technol.* **1994**, *2*, 35.
[195] R. H. Sui, A. S. Rizkalla, P. A. Charpentier, *Langmuir* **2006**, *22*, 4390.
[196] T. Brankova, V. Bekiari, P. Lianos, *Chem. Mater.* **2003**, *15*, 1855.
[197] E. Stathatos, P. Lianos, U. Lavrencic-Stangar, B. Orel, *Adv. Mater.* **2002**, *14*, 354.
[198] N. Steunou, F. Robert, K. Boubekeur, F. Ribot, C. Sanchez, *Inorg. Chim. Acta* **1998**, *279*, 144.
[199] D. Jiang, Y. Xu, B. Hou, D. Wu, Y. H. Sun, *Eur. J. Inorg. Chem.* **2008**, 1236.
[200] X. L. Li, Q. Peng, J. X. Yi, X. Wang, Y. D. Li, *Chem. Eur. J.* **2006**, *12*, 2383.
[201] B. Mukherjee, C. Karthik, N. Ravishankar, *J. Phys. Chem. C* **2009**, *113*, 18204.
[202] A. Zdravkov, J. Kudryashova, A. Kanaev, A. Povolotskiy, A. Volkova, E. Golikova, N. Khimich, *Mater. Chem. Phys.* **2015**, *160*, 73.
[203] K. Bernal Ramos, G. Clavel, C. Marichy, W. Cabrera, N. Pinna, Y. J. Chabal, *Chem. Mater.* **2013**, *25*, 1706.
[204] E. Rauwel, G. Clavel, M. G. Willinger, P. Rawel, N. Pinna, *Angew. Chem. Int. Ed.* **2008**, *47*, 3592; *Angew. Chem.* **2008**, *120*, 3648.
[205] M. Fujiwara, H. Wessel, H. S. Park, H. W. Roesky, *Chem. Mater.* **2002**, *14*, 4975.
[206] P. Arnal, R. J. P. Corriu, D. Leclercq, P. H. Mutin, A. Vioux, *J. Mater. Chem.* **1996**, *6*, 1925.
[207] G. Q. Guo, J. K. Whitesell, M. A. Fox, *J. Phys. Chem. B* **2005**, *109*, 18781.
[208] D. Caruntu, K. Yao, Z. X. Zhang, T. Austin, W. L. Zhou, C. J. O'Connor, *J. Phys. Chem. C* **2010**, *114*, 4875.
[209] G. Clavel, M. G. Willinger, D. Zitoun, N. Pinna, *Adv. Funct. Mater.* **2007**, *17*, 3159.
[210] E. Della Gaspera, A. S. R. Chesman, J. van Embden, J. J. Jasieniak, *ACS Nano* **2014**, *8*, 9154.
[211] X. H. Zhong, Y. Y. Feng, Y. L. Zhang, I. Lieberwirth, W. G. Knoll, *Small* **2007**, *3*, 1194.
[212] I. Bilecka, L. Luo, I. Djerdj, M. D. Rossell, M. Jagodic, Z. Jaglicic, Y. Masubuchi, S. Kikkawa, M. Niederberger, *J. Phys. Chem. C* **2011**, *115*, 1484.
[213] L. Luo, K. Hafliger, D. Xie, M. Niederberger, *J. Sol–gel Sci. Technol.* **2013**, *65*, 28.
[214] L. Luo, M. D. Rossell, D. Xie, R. Erni, M. Niederberger, *ACS Sustainable Chem. Eng.* **2013**, *1*, 152.
[215] D. Ito, S. Yokoyama, T. Zaikova, K. Masuko, J. E. Hutchison, *ACS Nano* **2014**, *8*, 64.
[216] Y. Z. Jin, Q. Yi, Y. P. Ren, X. Wang, Z. Z. Ye, *Nanoscale Res. Lett.* **2013**, *8*, 153.
[217] C. Liu, T. J. Hajagos, D. T. Chen, Y. Chen, D. Kishpaugh, Q. B. Pei, *ACS Appl. Mater. Interfaces* **2016**, *8*, 4795.
[218] Z. H. Zhang, M. H. Lu, H. R. Xu, W. S. Chin, *Chem. Eur. J.* **2007**, *13*, 632.
[219] Z. H. Zhang, X. H. Zhong, S. H. Liu, D. F. Li, M. Y. Han, *Angew. Chem. Int. Ed.* **2005**, *44*, 3466; *Angew. Chem.* **2005**, *117*, 3532.
[220] J. Chang, E. R. Waclawik, *Crystengcomm* **2012**, *14*, 4041.
[221] A. S. Skapin, L. Skrlep, D. Suvorov, V. Zunic, S. D. Skapin, *RSC Adv.* **2015**, *5*, 26769.
[222] N. Steunou, F. Ribot, K. Boubekeur, J. Maquet, C. Sanchez, *New J. Chem.* **1999**, *23*, 1079.
[223] S. C. Goel, M. Y. Chiang, P. C. Gibbons, W. E. Buhro, *Mater. Res. Soc. Symp. Proc.* **1992**, *271*, 3.
[224] G. Garnweitner, M. Antonietti, M. Niederberger, *Chem. Commun.* **2005**, 397.
[225] B. Liu, L. M. Liu, X. F. Lang, H. Y. Wang, X. W. Lou, E. S. Aydil, *Energy Environ. Sci.* **2014**, *7*, 2592.
[226] G. Garnweitner, Dissertation, University of Potsdam (Germany), **2005**.
[227] I. Djerdj, G. Garnweitner, D. S. Su, M. Niederberger, *J. Solid State Chem.* **2007**, *180*, 2154.
[228] G. Garnweitner, J. Hentschel, M. Antonietti, M. Niederberger, *Chem. Mater.* **2005**, *17*, 4594.
[229] B. C. Gaskins, J. J. Lannutti, *J. Mater. Res.* **1996**, *11*, 1953.
[230] M. Niederberger, G. Garnweitner, *Mater. Res. Soc. Symp. Proc.* **2005**, *879E*, Z9.8.1 (5 pages).
[231] D. Erdem, Y. Shi, F. J. Heiligtag, A. C. Kandemir, E. Tervoort, J. L. M. Rupp, M. Niederberger, *J. Mater. Chem. C* **2015**, *3*, 9833.
[232] Y. Wu, H. M. Liu, B. Q. Xu, Z. L. Zhang, D. S. Su, *Inorg. Chem.* **2007**, *46*, 5093.
[233] N. Kränzlin, M. Staniuk, F. J. Heiligtag, L. Luo, H. Emerich, W. van Beek, M. Niederberger, D. Koziej, *Nanoscale* **2014**, *6*, 14716.
[234] Z. Q. Li, W. C. Chen, F. L. Guo, L. E. Mo, L. H. Hu, S. Y. Dai, *Sci. Rep.* **2015**, *5*, 14178.
[235] E. R. Beach, K. Shqau, S. E. Brown, S. J. Rozeveld, P. A. Morris, *Mater. Chem. Phys.* **2009**, *115*, 371.
[236] L. Bahrig, S. G. Hickey, A. Eychmuller, *Crystengcomm* **2014**, *16*, 9408.
[237] V. K. Ivanov, P. P. Fedorov, A. Y. Baranchikov, V. V. Osiko, *Russ. Chem. Rev.* **2014**, *83*, 1204.
[238] C. J. Dalmaschio, C. Ribeiro, E. R. Leite, *Nanoscale* **2010**, *2*, 2336.
[239] W. Q. Lv, W. D. He, X. N. Wang, Y. H. Niu, H. Q. Cao, J. H. Dickerson, Z. G. Wang, *Nanoscale* **2014**, *6*, 2531.
[240] Y. Q. Liu, Y. Zhang, J. Wang, *Crystengcomm* **2014**, *16*, 5948.
[241] H. Cölfen, M. Antonietti, *Mesocrystals and Nonclassical Crystallization*, Wiley, Hoboken, **2008**.
[242] F. J. Heiligtag, M. D. Rossell, M. J. Suess, M. Niederberger, *J. Mater. Chem.* **2011**, *21*, 16893.
[243] D. Koziej, A. Lauria, M. Niederberger, *Adv. Mater.* **2014**, *26*, 235.
[244] C. J. Dalmaschio, E. R. Leite, *Cryst. Growth Des.* **2012**, *12*, 3668.
[245] D. G. Stroppa, L. A. Montoro, A. Beltran, T. G. Conti, R. O. da Silva, J. Andres, E. Longo, E. R. Leite, A. J. Ramirez, *J. Am. Chem. Soc.* **2009**, *131*, 14544.
[246] D. G. Stroppa, L. A. Montoro, A. Beltran, T. G. Conti, R. O. da Silva, J. Andres, E. R. Leite, A. J. Ramirez, *Chem. Commun.* **2011**, *47*, 3117.
[247] J. F. Ye, W. Liu, J. G. Cai, S. A. Chen, X. W. Zhao, H. H. Zhou, L. M. Qi, *J. Am. Chem. Soc.* **2011**, *133*, 933.
[248] R. O. Da Silva, R. H. Goncalves, D. G. Stroppa, A. J. Ramirez, E. R. Leite, *Nanoscale* **2011**, *3*, 1910.
[249] J. Ba, A. Feldhoff, D. Fattakhova-Rohlfing, M. Wark, M. Antonietti, M. Niederberger, *Small* **2007**, *3*, 310.
[250] R. Buonsanti, E. Carlino, C. Giannini, D. Altamura, L. De Marco, R. Giannuzzi, M. Manca, G. Gigli, P. D. Cozzoli, *J. Am. Chem. Soc.* **2011**, *133*, 19216.
[251] M. Niederberger, M. H. Bartl, G. D. Stucky, *Chem. Mater.* **2002**, *14*, 4364.

[252] G. V. Jensen, M. Bremholm, N. Lock, G. R. Deen, T. R. Jensen, B. B. Iversen, M. Niederberger, J. S. Pedersen, H. Birkedal, *Chem. Mater.* **2010**, *22*, 6044.
[253] I. M. Grabs, C. Bradtmoller, D. Menzel, G. Garnweitner, *Cryst. Growth Des.* **2012**, *12*, 1469.
[254] I. C. Masthoff, M. Kraken, D. Mauch, D. Menzel, J. A. Munevar, E. B. Saitovitch, F. J. Litterst, G. Garnweitner, *J. Mater. Sci.* **2014**, *49*, 4705.
[255] I. C. Masthoff, M. Kraken, D. Menzel, F. J. Litterst, G. Garnweitner, *J. Sol–gel Sci. Technol.* **2016**, *77*, 553.
[256] M. V. Kovalenko, L. Manna, A. Cabot, Z. Hens, D. V. Talapin, C. R. Kagan, V. I. Klimov, A. L. Rogach, P. Reiss, D. J. Milliron, P. Guyot-Sionnnest, G. Konstantatos, W. J. Parak, T. Hyeon, B. A. Korgel, C. B. Murray, W. Heiss, *ACS Nano* **2015**, *9*, 1012.
[257] J. Owen, *Science* **2015**, *347*, 615.
[258] A. Nag, H. Zhang, E. Janke, D. V. Talapin, *Z. Phys. Chem. (Muenchen Ger.)* **2015**, *229*, 85.
[259] M. A. Boles, D. Ling, T. Hyeon, D. V. Talapin, *Nat. Mater.* **2016**, *15*, 141.
[260] B. I. Kharisov, H. V. R. Dias, O. V. Kharissova, A. Vazquez, Y. Pena, I. Gomez, *RSC Adv.* **2014**, *4*, 45354.
[261] J. H. Ba, J. Polleux, M. Antonietti, M. Niederberger, *Adv. Mater.* **2005**, *17*, 2509.
[262] K. Fominykh, J. M. Feckl, J. Sicklinger, M. Doblinger, S. Bocklein, J. Ziegler, L. Peter, J. Rathousky, E. W. Scheidt, T. Bein, D. Fattakhova-Rohlfing, *Adv. Funct. Mater.* **2014**, *24*, 3123.
[263] L. Luo, D. Bozyigit, V. Wood, M. Niederberger, *Chem. Mater.* **2013**, *25*, 4901.
[264] K. Fominykh, P. Chernev, I. Zaharieva, J. Sicklinger, G. Stefanic, M. Doblinger, A. Muller, A. Pokharel, S. Bocklein, C. Scheu, T. Bein, D. Fattakhova-Rohlfing, *ACS Nano* **2015**, *9*, 5180.
[265] Y. J. Liu, J. M. Szeifert, J. M. Feckl, B. Mandlmeier, J. Rathousky, O. Hayden, D. Fattakhova-Rohlfing, T. Bein, *ACS Nano* **2010**, *4*, 5373.
[266] K. Peters, P. Zeller, G. Stefanic, V. Skoromets, H. Nemec, P. Kuzel, D. Fattakhova-Rohlfing, *Chem. Mater.* **2015**, *27*, 1090.
[267] J. M. Szeifert, J. M. Feckl, D. Fattakhova-Rohlfing, Y. J. Liu, V. Kalousek, J. Rathousky, T. Bein, *J. Am. Chem. Soc.* **2010**, *132*, 12605.
[268] A. Aboulaich, B. Boury, P. H. Mutin, *Eur. J. Inorg. Chem.* **2011**, 3644.
[269] S. X. Zhou, G. Garnweitner, M. Niederberger, M. Antonietti, *Langmuir* **2007**, *23*, 9178.
[270] Y. Q. Hu, S. X. Zhou, L. M. Wu, *Polymer* **2009**, *50*, 3609.
[271] S. X. Zhou, *L. M. Wu, Macromol. Chem. Phys.* **2008**, *209*, 1170.
[272] A. Kockmann, J. Hesselbach, S. Zellmer, A. Kwade, G. Garnweitner, *RSC Adv.* **2015**, *5*, 60993.
[273] C. Grote, K. J. Chiad, D. Vollmer, G. Garnweitner, *Chem. Commun.* **2012**, *48*, 1464.
[274] J. De Roo, F. Van den Broeck, K. De Keukeleere, J. C. Martins, I. Van Driessche, Z. Hens, *J. Am. Chem. Soc.* **2014**, *136*, 9650.
[275] J. De Roo, Y. Justo, K. De Keukeleere, F. Van den Broeck, J. C. Martins, I. Van Driessche, Z. Hens, *Angew. Chem. Int. Ed.* **2015**, *54*, 6488; *Angew. Chem.* **2015**, *127*, 6588.
[276] M. L. H. Green, *J. Organomet. Chem.* **1995**, *500*, 127.
[277] M. Niederberger, G. Garnweitner, F. Krumeich, R. Nesper, H. Colfen, M. Antonietti, *Chem. Mater.* **2004**, *16*, 1202.
[278] J. De Roo, S. Coucke, H. Rijckaert, K. De Keukeleere, D. Sinnaeve, Z. Hens, J. C. Martins, I. Van Driessche, *Langmuir* **2016**, *32*, 1962.
[279] J. De Roo, K. De Keukeleere, Z. Hens, I. Van Driessche, *Dalton Trans.* **2016**, *45*, 13277.
[280] J. De Roo, E. A. Baquero, Y. Coppel, K. De Keukeleere, I. Van Driessche, C. Nayral, Z. Hens, F. Delpech, *ChemPlusChem* **2016**, *81*, 1216.
[281] R. O. da Silva, T. G. Conti, A. F. de Moura, D. G. Stroppa, L. C. G. Freitas, C. Ribeiro, E. R. Camargo, E. Longo, E. R. Leite, *ChemPhysChem* **2009**, *10*, 841.

Manuscript received: December 21, 2016
Accepted manuscript online: April 4, 2017
Version of record online: May 26, 2017